Yale University

Physics Department
P.O. Box 6666
New Haven, Connecticut 06511

Campus address:
217 Prospect Street

October 2, 1984

Dr. Leon M. Lederman, Director
Fermi National Accelerator Laboratory
P.O. Box 500
Batavia, Illinois 60510

Dear Leon:

We are writing to transmit the enclosed proposal "A High Sensitivity Study of Beauty and Charm in Hadroproduction at the Tevatron".

As is detailed in the proposal, and in our letter of intent of May 7, 1984, we would like to initiate a program of heavy quark studies at the TEVATRON. The proposed experiment is, in our view, a necessary first phase in that program. It will provide essential physics data such as the cross section and characteristics of Beauty hadroproduction, and it will provide experience with two new experimental tools for heavy quark physics - the holographic, diffusion suppressed streamer chamber, and the fast, high P_T, electron trigger system using a tracking TRD and a special processor.

Future experiments would involve the use of other beams (K's, n's, γ's) and the upgrade of the downstream spectrometer capabilities. This upgrade could be accomplished by moving the unique elements to an existing spectrometer or to a new spectrometer which has been specifically designed for the "next" generation of experiments.

We believe that the streamer chamber development program has demonstrated the techniques necessary to construct the chamber. However, we realize that we have not yet demonstrated a chamber which has all of the resolution parameters we require. We also realize that the present collaboration is not large enough to carry out the proposed experiment. We therefore are requesting that the laboratory approve our experiment subject to two conditions.

1. That we demonstrate a streamer chamber with track width ~30μm, with 15-20 streamers/mm, which operates at ~60 atmospheres.

2. That we form a collaboration of sufficient size and strength to build the experiment and to analyze the data in a timely fashion.

We expect to achieve these "milestones" by the summer of 1985.

Although approval at this time would be conditional, it is still important for two reasons. Firstly, in the present climate, many potentially interested groups are reluctant to undertake an experimental

program without some indication that it will receive laboratory support and beam time. Secondly, the support for the goals of our program, which such approval would provide, is needed to obtain the funding required to complete the construction of the chamber.

The time scale we envisage for the experiment (assuming that we do obtain the requested conditional approval) is as follows:

Present → June 1985	Complete the test version of the streamer chamber (see proposal section 3.2) and perform "milestone" tests. Build collaboration and carry on design of downstream equipment.
June 1985	Approval becomes "unconditional", construction of the full sized chamber and the downstream equipment begins.
May 1986	Install streamer chamber and parts of the downstream system in the beam at FNAL and run for ~1-2 months to commission the chamber, provide film for testing the analysis equipment and to commission the beam and the downstream equipment which is available.
January 1987	Installation of experiment is complete and experimental run begins.

We belive we can meet this schedule and that it represents a timely introduction of a new and promising approach to heavy quark physics at the TEVATRON. We would, of course, be happy to provide any future information desired.

Sincerely,

Richard D Majka

Richard D. Majka

Jack Sandweiss

Jack Sandweiss
Correspondents

P. Lucas, M. Johnson
Fermilab

R. Beringer, S. Dhawan, A. Disco,
J. Hissong, R.D. Majka, J. Sandweiss
A.J. Slaughter, L. Teig, and E. Wolin
Yale University

S. Tavernier
Inter University Institute
for High Energy
Vrije Univeriteit Brussel

Fermilab Proposal No. 755

A HIGH SENSITIVITY STUDY OF BEAUTY AND CHARM IN HADROPRODUCTION AT THE TEVATRON

P. Lucas, M. E. Johnson
Fermilab
Batavia, IL

S. Tavernier
Inter University Institute for High Energy Physics
Vrije Universiteit
Brussels, Belgium

R. Beringer, S. Dhawan, A. Disco, J. Hissong,
R. D. Majka, P. Olivier, J. Sandweiss,
A. J. Slaughter, L. Teig, E. Wolin
Yale University
New Haven, CT

Correspondents: J. Sandweiss,R. Majka
Physics Dept., Yale University
260 Whitney Ave.
Box 6666
New Haven CT 06511
(203) 436-4890

Table of Contents

List of Figures

List of Tables

A HIGH SENSITIVITY STUDY OF BEAUTY AND CHARM IN HADROPRODUCTION AT THE TEVATRON

1. Introduction

We present a proposal for a systematic approach to beauty and charm physics at the Tevatron using a high resolution streamer chamber and an open geometry downstream spectrometer. The experience of this collaboration[1] has convinced us that Tevatron II provides an excellent and in many ways unique opportunity for heavy quark studies, provided that the proper experimental techniques can be found. We believe these entail:

1. A high resolution vertex detector with powerful pattern recognition capabilities. This requires a single track RMS resolution on the order of 5 μm, two track resolution less than ~50 μm, and a large number of points on each track over a sufficently long distance.
2. A powerful downstream spectrometer.
3. A triggerable system with a sensitivity of at least a few events per nanobarn.

There is now wide agreement on the need for a suitable vertex detector for charm and beauty physics. No currently existing detector is ideal in all respects, but we are convinced that the streamer chamber approach has major advantages in beauty physics and is complementary to other approaches for charm physics. Advances in streamer chamber technology[2] by both the Yale group and Munich/CERN (V. Eckhardt et al.) have made an appropriate chamber feasible. A holographic streamer chamber with diffusion suppression is a triggerable device with high resolution (track width

---

[1] SPS NA25, SLAC BC 72/73, Fermilab E490 and E630

[2] see section below and Appendix

·30μm, setting error ~5 μm) over a large volume of space (15 x 5 x 1.5 cm^3). It operates at high pressure (60 atm) providing a target with density comparable to liquid hydrogen so that high interaction rates are obtainable. The information content per track in the form of X-Y-Z space points is very large. Its major disadvantages - a long recovery time and the need to measure events on film - can both be overcome by a sufficently selective trigger and the appropriate use of the downstream spectrometer data.

This proposal covers Phase I of what we envision as major program of heavy quark physics. In this phase we will concentrate on beauty hadroproduction. The apparatus (see Figure 3-1 and section 3) will consist of incident beam tagging chambers, the streamer chamber, a magnetic pectometer, a tracking TRD, a lead glass electromagnetic calorimeter, and a fast trigger processor. The system will be triggered on a high P_T electron using the information from the TRD and the calorimeter to obtain a on-line beauty enhancement factor of 218. This detector will be capable of collecting ~350 beauty and ~49,000 charm events when exposed to a beam of 1.5 Mhz of 800 Gev/c protons for 1000 hours. Although the downstream spectrometer is modest for Phase I, this sample will allow studies of B particle hadroproduction, B^o and $B^{\pm}$ lifetimes, and several high statistics studies in the charm system. We envision this Phase I experiment as the begining of a substantial program of heavy quark physics at the Tevatron based on the unique capabilities of the high resolution streamer chamber.

2. Physics

The experiment we propose is a first step in a new program to study heavy quark physics, especially b quark physics in fixed target experiments. Before detailing the specific aims of the proposed experiment, we review the reasons for our belief in the importance of this area of research.

The study of heavy quark physics in fixed target experiments offers the potential to resolve fundamental questions in elementary particle physics which are difficult to answer at e^+-e^- colliders. In our view, the past dominance of collider experiments in this field reflects, in part, the time required to develop the new technology needed to deal with the special problems of fixed target experiments. It would be a mistake to assume that that situation will continue in the future and to miss the special and exciting potential of the fixed target approach. The main advantages of fixed target experiments are:

- rate
- eclectic production of all varieties of heavy quark systems, particularly with the use of nucleon, pion, kaon, and hyperon incident beams,
- associated production, allowing unbiased studies of the "non-trigger" particle,(we note that associated production is not the same as pair production such as occurs predominantly in e^+-e^- collisions)
- accessibility of both production and decay vertices.

Among the most fundamental questions that can be tested in an experiment such as we are proposing is the validity of the six quark picture within the framework of the K-M theory of the electro-weak quark couplings. This picture is intimately related to our view of the quarks and leptons as a family of generations, and its careful testing is one of the exerimental

avenues open to us to study the generation question. Thus the elements of the K-M matrix need to be overdetermined to see if the overall experimental situation is consistent with the picture. A number of measurements are required. First, the individual B particle lifetimes need to be accurately determined. Second the striking predictions [1] of large mixing in the B_s^o system must be tested. Similarly, the $D^o\bar{D}^o$ mixing should be studied with a sensitivity substantially better than the simple four quark [2] estimate of $\sim 10^{-3}$ even if the K-M prediction of $\sim 10^{-7}$ cannot be reached. Finally, the rate for B particle decays to systems of ordinary (i.e. non charmed) quarks must be determined.

The study of the B particle systems have great potential for improving our knowledge of the nature and origin of CP violation. Branching ratio tests, testing the equality of the rates for B versus $\bar{B}$ decay to conjugate channels, as well as the neutral meson phenomena analagous to those in the K^o system may show CP violation effects. In the K-M picture, branching ratio differences for B versus $\bar{B}$ decay vanish to first order for the dominant decay modes but can be appreciable (~10%) for other channels such as those involving b-->u decay. As noted above, we do not yet know even the rate of b-->u decays (although we have an upper limit of $\Gamma(b\text{-->}u) = \lesssim .05\Gamma(b\text{-->}c)$.

Clearly, CP studies will not be possible in the experiment proposed here, and indeed, they appear to be difficult with the streamer chamber technique. Experiments to study CP effects will have to be very specifically and carefully designed electronic experiments. However, the formation to be gained from the program we propose will be essential for

the design of such experiments.

The hadroproduction of heavy quark systems is a subject of fundamental interest in its own right, as well as an essential tool in the exploitation of the Tevatron for heavy quark physics. The excited states which decay strongly into the stable B's, D's, etc. are of considerable interest from a phenomenological point of view. Similarly, the study of particles with two heavy quarks (e.g. ccu, etc.) is both analogous with and complimentary to the study of the charmonium and upsilon systems.

Finally, the field of heavy quark physics is relatively unstudied, especially with regard to the wide variety of states expected in hadro-production. There is, therefore, the possibility of surprises, which are by definition, unexpected, but which have historically occured with sufficient frequency to justify our practice of insisting on a careful and comprehensive experimental base for our theoretical conclusions.

As noted above, the experiment proposed here cannot address all of these issues. It does, however, address a number of key questions which are detailed below.

2.1. Observation of Hadronically Produced B Particles and Determination of the Production Cross Section

Based on the central $B\bar{B}$ production model described in the section on rates, the assumption of a 50 nb production cross section in nucleon-nucleon collisions, and an $A^{2/3}$ variation of the production cross section with atomic weight (A) of the target, we expect 350 $B\bar{B}$ events in our triggered sample of pictures: this corresponds to a sensitivity of 7

etected $B\bar{B}$ events per nb of production cross section.

As is discussed in the section on analysis, a conservative estimate is that we will be able to identify 50% of the $B\bar{B}$ events in the triggered sample if the B lifetime is $\sim 10^{-12}$ secs. Further we expect to be able to associate B decay tracks with their parents with high efficiency. Then, using the information from the downstream spectrometer (after having "linked" tracks in the streamer chamber with tracks in the spectrometer) we will be able to determine the charge states of the $B\bar{B}$ pair.

If the B lifetime is shorter than 10^{-12} sec. the experiment will still have considerable sensitivity. In particular, the trigger electron in a B event will not be compatible with the daughter charmed particle decay vertex. In the extreme case where the B lifetime is zero, a conservative evaluation using the Monte Carlo shows that $B\bar{B}$ events can be identified in 10% of the $B\bar{B}$ triggered pictures leading to a sensitivity of 1.4 events/nb of total hadroproduction cross section. In this case our experiment cannot determine the charge state of the $B\bar{B}$ system.

2.2. Measurement of B Particle Lifetimes

The most straightforward method to measure B particle lifetimes in our experiment is to use a miss distance analysis of the trigger electron. Because of the high P_T cut (~1 GeV/c) in the trigger, the electron which triggers the event is essentially always the product of the leptonic decay of a B particle rather than of the leptonic decay of a daughter charmed particle. The miss distance, S, is defined as shown in Fig. 2-1. It can be shown [3] that the mean miss distance $\langle S \rangle$ is uniquely related to the

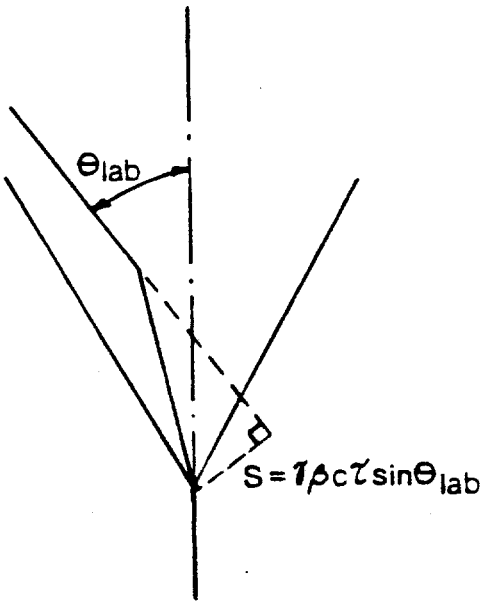

Figure 2-1: Sketch Showing Definition of Miss Distance S.

proper lifetime τ of the decaying particle and approximately equal to $c\tau_0$.

For B particle lifetimes of $\sim 10^{-12}$ sec. the miss distance will be measured to an average fractional accuracy of 5% so that the final lifetime errors will be dominated by the statistical error. As noted above we will be able to identify $\geq$50% of the $B\bar{B}$ triggered events, and be able to determine the charge state of the $B\bar{B}$ system. Thus, assuming our "canonical" 50 nb and equal numbers of charged and neutral B's we would have 1/2 x1/2 x 350 = 88 events in each sample. The resulting charged and neutral lifetimes will then be determined with a standard deviation of ~10% of the lifetime.

Finally, the discussion of the miss distance analysis should not leave the impression that we are unable to reconstruct the topology of the B decay vertices. Indeed, low statistics Monte Carlo studies indicate that a substantial fraction of the events can be comletely reconstructed topologically. We are still in the process of refining this rather complex analysis procedure and thus have used the more straightforward miss distance method for estimating the accuracy with which we can measure lifetimes. The question of complete reconstruction is discussed in more detail in the section on data analysis.

2.3. Phenomenology of B Particle Production

As noted in the analysis section, $B\bar{B}$ events will be complex. The techniques for reconstructing the events and establishing the correct topology of decay chains in the events is still evolving and will involve both spectrometer data and measurements of the picture in an integrated way. For the purposes of this proposal we have taken a conservative point of view, verified by our Monte Carlo simulations, that we will be able to

identify 50% of the triggered $B\bar{B}$ events and to correctly assign (decay) tracks to the parent B including the daughter tracks from the D decay. In most of these events the charm vertices can be unambiguously reconstructed but only in a fraction of the events can the B vertex be uniquely located if only the two dimensional projected data in the plane of the streamer chamber window are used. Since we have carefully studied the reconstruction with the XZ data only, we will not assume here that B vertices will be precisely located. Since 3-D measurements are available in the chamber, and since downstream data on momenta, effective masses, etc. are available, we believe that we will be able to topologically fully reconstruct a large fraction of the events.

Nevertheless, even with the more limited information assumed above, considerable information on the B particle production can be obtained. For example the visible P_T and x distributions can be measured. These are determined from the total momentum and transverse momentum of all the final charged decay products from a B particle. These visible P_T and x distributions are closely related to the true distributions which can be found via deconvolution using a Monte Carlo simulation.

The visible P_T and x distributions can also be separately measured for B^o, $\bar{B}^o$, B^+, and B^- particles and compared. The dynamical characteristics (multiplicities, P_T and x distributions, etc.) of the particles produced with the $B\bar{B}$ pair can also be measured.

2.4. Mixing in the Neutral B System

Although it is clearly premature to expect to observe $B^0\bar{B}^0$ mixing at a time when not even the total hadroproduction cross section is known, it is interesting to estimate what might be observed given the assumptions that are reasonable at this time.

The only way this experiment can determine the B^0 versus $\bar{B}^0$ character of a decaying neutral B state is by the leptonic decay. (Note that B^0 states yield e^-, etc). To know the character of the neutral B at the instant of its production requires knowing the particle versus antiparticle character of the other B particle in the event. Events of interest for mixing studies will be those in which the trigger electron or positron arises from a neutral B decay and in which the particle (antiparticle) character of the other B can be determined. This can clearly be done if the "other" B is a B^0 which decays leptonically or is a charged B.

We now estimate the number of events we might observe in which we could determine that mixing had occured.

Assume our "canonical" 50 nb production cross section, $A^{2/3}$ depenence and other parameters as detailed in the section on rates. We then trigger on 350 $B\bar{B}$ events. Of these, we have determined $\geq$ 50% will be identifiable as $B\bar{B}$ events. The resulting sample of 175 events should contain 87 events in which the trigger electron originated in a neutral B decay. Of these events, the other B is charged in half the cases, or 43 events. All of these 43 are useful for the mixing analysis.

The B_s^o is expected [1] to have a mixing parameter R between 0.4 and 0.85. If we assume that 10% of the neutral B's are B_s^o and the rest B_d^o, then ~5 events out of the 43 should be B_s^o. Then (neglecting the mixing in B_d^o) we would expect between 2 and 4 mixed events.

Despite the meager statistics, such events could be quite significant because of the ability of the streamer chamber to measure decay distances. It is easy to show [1] that if (as expected) the long and short lifetimes in the B_s^o system are nearly equal (i.e., their difference small compared to their magnitude τ_o) then the time distribution of the "mixed" decays is of the form

$$\frac{dN}{dt} \sim t^2 \, e^{-t/\tau_o} \qquad (1)$$

As a consequence of 1, half of all the mixed decays occur beyond $t = 2\tau_o$. Thus a few events could be significant because their time distribution offers a powerful means of rejecting background events which should have the usual exponential decay distribution.

It is clear that a second generation experiment with the high resolution streamer chamber could be designed to make a definitive test of B_s^o mixing.

2.5. Physics With a Trigger Sample of 49,000 Charm Pair Events

A number of interesting measurements in charm physics are possible with this large sample even though our experiment does not have charged particle identification (apart from the excellent electron identification), fine grained electromagnetic calorimetry, or hadron calorimetry.

2.5.1. Test of $\Gamma(D^+ \to eX\nu) = \Gamma(D^0 \to eX\nu)$. Measurements of Branching Ratios and Lifetimes

As has been recognized since the early days of charm physics, the structure of the Cabibbo allowed part of the semileptonic Lagrangian [2] (which carries zero isotopic spin) predicts the equality of the semileptonic rates of D^0 and D^+ when the hadronic part of the decay is an isospin 1/2 state such as $\bar{K}^0$, K^- or K^{*-}. In other words, for Cabibbo allowed decays, semileptonic decay rates are equal. This also means that down to the level (~5%) at which Cabibbo suppressed decays occur, the total semileptonic rates for D^0 and D^+ should be equal. This is one of the cleanest predictions of the theory and should be tested carefully. We note that current comparisons of lifetimes and branching ratios have large errors.

The present experiment is particularly well suited to carry out this test in that we can measure, in the same exeriment, the ratio of D^+ and D^0 (or D^- and $\bar{D}^0$) branching ratios <u>and</u> the ratio of D^0 and D^+ lifetimes. The test is then of the form

$$\frac{BR(D^0 \to eX\nu)}{BR(D^+ \to eX\nu)} = \frac{\tau(D^0)}{\tau(D^+)}$$

In taking the ratio of ratios many of the systematic errors cancel out. The lifetimes will be measured with negligible statistical error and we estimate systematic errors of a few percent (still under study) in the lifetime determinations.

The branching ratios are measured by observing the electronic decay of the other (non trigger) D particle. A conservative estimate of the probability that an electron from the non trigger D will be so identified by our apparatus is 15%.

In half (25,500) of the observed sample the non trigger D will be a D^o. Using the latest measurement of the D^o semileptonic branching ratio [4] of .06 ± .02 ±.02 we obtain 1530 D^o electron decays of which 15%, or 230, will be identified by our apparatus. The branching ratio for D^+ is .17 ± .03 ± .03 [4] leading to an identified sample of 650 decays. Thus we should have a statistical standard deviation in the ratio of branching ratios of less than 10%.

2.5.2. Measurement of the $D\bar{D}$ Hadronic Production Cross Section

Although other experiments currently under way will make measurements of the hadronic cross section, our experiment will make an important contribution to the subject. We will have the low systematic errors of the high resolution bubble chamber experiment and the statistical power of the proposed purely electronic experiments with solid state vertex detection.

The large data sample will allow us to use the "all charged" decay modes to completely determine the momenta of the charged and neutral D's. The

fraction of all charged modes is ~10% for both D^+ and D^0 so that about 2500 fully reconstructed events in each of the D^0 and D^+ samples can be expected.

2.5.3. Search for Higher Mass Charm Resonances Decaying into D or $\overline{D}$

The ~5000 kinematically determined events can be used to search for the production of resonances which decay into D or $\overline{D}$. One would certainly expect to find the D^* and determine its production cross section. The size of the event sample would suggest that a significant search for other states of higher mass or more complex decay characteristics will be possible.

2.5.4. Measurement of F-Meson Production

The rate of F meson production in hadronic collisions is unknown at this time. We assume that F production is 10% of the charm production giving 4900 F events in the trigger sample. The estimate of 10% is consistent with the limit in p-p interactions from LEBC.

Our experiment can search for F meson production in two ways. First, the lifetime spectrum of charged charmed particles can be analyzed into two components due to $D^{\pm}$ and F. This approach could use the miss distance distribution or the flight path length corrected to approximate proper time using the total visible momentum from the decay. Given the current substantial differences between the $F^{\pm}$ and $D^{\pm}$ lifetimes [5] and the expected high statistics, this approach should be successful. Monte Carlo studies to estimate the sensitivity are under way.

One difficulity with this approach is that the Λ_c^+ has approximately the same lifetime as the F. Data from LEBC on Λ_c^+ production indicate that the Λ_c^+ has a considerably flatter x_f distribution and could be kinematically separated from the (presumed) central F production. Quantitative studies of this question are underway.

A second approach uses the decay

$$F^{\pm} \dashrightarrow \phi^{o}\pi^{\pm}$$
$$\phi^{o} \dashrightarrow K^{+}K^{-}$$

Estimates for the branching ratio for this this decay mode range between 4% and 10%. Assuming 5% and recalling that the branching ratio for $\Phi \dashrightarrow K^+K^-$ is 49%, we estimate there will be 119 events of this type. The events should be very clean; the background is due only to $D^{\pm} \dashrightarrow K^{\pm}\pi^{\pm}\pi^{\pm}$. Even though K's are not identified as such in our spectrometer, the Φ peak in K^+K^- is easily seen as demonstrated by the CLEO group at CESR in their analysis of F production [6].

3. Apparatus

The trigger for the high resolution streamer chamber must be sophisticated enough to provide the rate reduction to < 10 Hz and must be generated within the few microsecond memory time of the chamber. Also, because the output of the chamber is recorded on film, the trigger must substanially enrich the fraction of events with heavy quarks if the scanning and measuring is not to become intolerably burdensome.

In the design of the Phase I spectrometer, we have focussed on this trigger requirement. Information from a tracking transition radiation detector (TRD) will be combined with that from a lead glass electromagnetic calorimeter with the help of a fast processor to determine that the event contains a high P_T electron characteristic of heavy quark decay. Because the streamer chamber, tracking TRD, and processor are essential, state of the art devices, we plan to concentrate on fabricating, testing, and incorporating these devices into the experiment. For the remainder of the apparatus, the PWC's and electromagnetic calorimeter, we will borrow heavily from existing systems. Once the goals of this proposal with respect to streamer chamber performance and trigger rates are meet, we anticipate the addition of particle identification, fine grained electromagnetic calorimetry, hadron calorimetry and other features to the spectrometer. This upgrade could be accomplished by moving the streamer chamber and specialized trigger devices to another spectrometer.

3.1. The Spectrometer

The experimental arrangement is sketched in Fig. 3-1.

Table 3-1 lists the various elements, their dimensions transverse to the beam (X,Y) and their position along the beam (Z).

The trajectory of the incident particle is measured in a set of beam chambers (PB1-PB3). The streamer chamber has a sensitive region 5cm wide, 1.5cm high and 15cm along the beam and is filled with 60 atmospheres of a 90% Neon, 10% Helium gas mixture. In addition to providing high resolution tracking (30 μm wide tracks, 5 μm setting error), it serves as a .5% interaction length target. The chamber itself is described in detail in the second part of this section. Recent progress in "storing" the ionization electrons on oxygen molecules to reduce the track width due to diffusion of the primary ionization electrons as well other aspects of the streamer chamber development program are described in Appendix III.

Multiwire proportional chambers provide basic particle tracking in the magnetic spectrometer (chambers P1-P6). Each chamber provides X-U-V information with a vertical plane of wires and two additional planes oriented at ± 20° to the vertical. The wire spacing is 1mm in the smaller upstream chambers and 2mm in the larger chambers (1m x 2m) downstream of the spectrometer magnet. The system contains a total of 12,000 wires.

The directions of charged particles leaving the streamer chamber are measured in the PWC's P1-P3 to .19 mrad (standard deviation) in the horizontal(bending) plane and .65 mrad in the vertical plane. This will

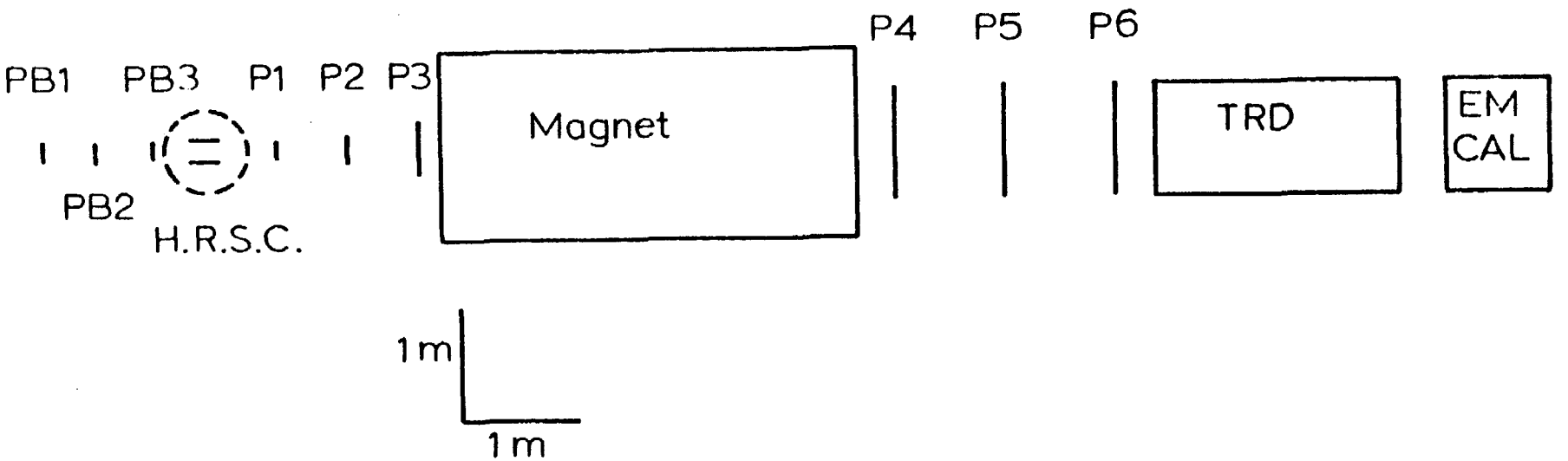

Figure 3-1: Diagram of apparatus

Table 3-1: Size and position along the beam line of the elements of the apparatus. X is transverse to the beam, Y is vertical, and Z is along the beam. The magnet bends horizontally.

Element	Position along Beam (meters)	Dimensions Transverse to Beam (meters)	
	Z	X	Y
Beam Tagging Chambers			
Streamer chamber	0.0	± .0275	± .010
P1	.6	± .0625	± .0625
P2	1.25	± .125	± .125
P3	1.9	± .25	± .25
Magnet(front)	2.0	± .75	± .75
Magnet(back)	5.5	± .75	± .75
P4	5.8	±1	± .5
P5	6.8	±1	± .5
P6	7.8	±1	± .5
TRD 1	8.0	±1	± .5
2	8.5	±1	± .5
3	9.0	±1	± .5
4	9.5	±1	± .5
5	10.0	±1	± .5
Electromagnetic Calorimeter	10.5	±1	± .5

allow matching to the directions of tracks measured in the streamer chamber, determined to approximately 0.1 mrad. A typical inelastic event will have ten charged particles in a ± 50 mrad angular cone about the beam resulting in an angular separation of tracks typically 10 times larger than the resolution.

We will require a large aperture magnet, 1.5 meters horizontally with a 1.0 meter vertical gap, and have assumed in our design considerations that a 3.5 meter long magnet can provide a P_T kick of .7 GeV/c. Momenta are measured in the PWC spectrometer with a resolution $\sigma_p/P = 4.3 \times 10^{-4} \cdot P$.

The angular acceptance of the spectrometer at various positions along the beam both in the vertical (nonbending) plane and as a function of momentum in the horizontal (bending) plane are given in table 3-2.

Table 3-2: Charged particle acceptances (mrad).

	Bend Plane			Nonbend Plane
z(m)	3 GeV/c	10 GeV/c	20 GeV/c	
5.8 (at P4)	± 90	± 148	± 160	± 86
7.8 (at P6)	± 7	± 92	± 110	± 64
10.5 (EM cal)	0	± 50	± 73	± 48

Electrons are identified and their trajectories determined in a set of transition radiation detectors (TRD's); their total energy is measured in the lead-glass calorimeter. A fast parallel processor will be employed:

1. to find valid electron tracks in the TRD's and, coupled with a measurement of the transverse coordinates of the incident beam particle, determine the momentum P and the transverse momentum P_T of the particle
2. to require that the momentum agree with the total energy deposited in the lead glass along the trajectory
3. to check that P and P_T fall within the trigger cuts.

A description of the processor is presented in Appendix II.

For a number of reasons, transition radiation detectors are well matched to the requirements of the trigger. Since the intensity of transition

radiation depends only on the Lorentz factor γ of the particle, the device is ideally suited for distinguishing light electrons from heavy hadrons at very high energies. The x-rays are emitted with angles typically $1/\gamma \lesssim 0.2$ mrad for the 10-100GeV/c electrons of interest and therefore lie along the path of the particle, providing excellent position information. The detector does not disturb the electron, allowing subsequent precision measurement of the total energy. The system is compact (unlike gas Cerenkov detectors) thus minimizing the dimensions of the electromagnetic calorimeter. The information may be read out with the same system used for the central PWC spectrometer. Large TRD's have been built and successfully operated in this energy range. [7]

We plan to use a set of five identical TRD's, the first three to be used in the trigger and the last two to enhance the quality of the electron identification off-line as well as to increase the likelihood of observing two electrons in a charm or beauty event. The active area of each detector is 1m vertically by 2m horizontally with a central deadened region to allow the beam to pass unnoticed. Each radiator consists of a stack of polypropylene foils, perhaps two hundred 17 μm foils spaced 1 mm apart for a total thickness of 20cm, followed immediately by a Xenon-Methane filled proportional wire chamber. The anode plane consists of vertical wires (perpendicular to the magnetic bend plane) spaced every 2 mm. To provide true three-space track points with good ambiguity rejection, cathode signals are derived from 8 mm wide strips oriented at $\pm$ 20° to the anode wires. This geometry provides horizontal resolution of ~0.6mm for good momentum resolution and vertical resolution of ~4mm.

Good e-π discrimination in the TRD demands that the few 6-20keV transition radiation X-rays be recognized in the presence of ionization from comparable energy loss by the charged particle. Energy deposited in the chamber from an X-ray is localized in the chamber and produces a narrow pulse in time (~40 nsec) whereas the ionization due to energy loss is distributed across the entire interelectrode gap and is collected over 300-400 nsec. However, due to fluctuations and δ-rays, the size of the ionization 'pulse' is quite irregular, making it difficult to detect the X-rays on the basis of pulse height alone, particularly in a large multi-channel system. Substantially better and more stable X-ray detection is realized by the technique of 'cluster-counting'. After appropriate pulse shaping, the larger X-ray spikes may be more readily discriminated from the smaller ionization peaks. In this manner, we expect to detect electrons with ~90% efficiency per track while mistaking a hadron for an electron 10-15% of the time. [7]

By requiring signals in three detectors, the electron efficiency is 70% but the background due to hadrons faking electrons plummets to ~0.2% (hadron rejection of ~400). When coupled with the comparison of the particle momentum to the lead-glass energy, the overall hadron rejection should exceed a factor of 4000 as shown in the section on rates and backgrounds. Tracks in the TRD system are dominantly electrons and few in number, greatly reducing the burden on the fast trigger processor.

The electromagnetic calorimeter is constructed from 224 15cm x 15cm x 9 radiation length thick lead glass detectors (or the equivalent). Using two blocks in tandem to provide 18 radiation lengths along the particle

trajectory an area of 1.1m x 2.4m can be covered.

Energies of photons and electrons will be measured with a resolution (RMS):

$$\sigma_E/E = (2+4/\sqrt{E(GeV)})\%$$

By measuring the centroid of the energy profile the hit point can be determined to ± 1.8 cm, or the direction of the photon or electron to ±2 mrad. The photons from low energy neutral pions can be resolved spatially and identified as originating from a π^o via the two photon mass with a resolution of 8-25 MeV/c^2 (for momenta from 5-15 GeV/c). At higher energies, single clusters will be assumed to originate from neutral pions, with the energy and direction of the π^o then known with the above precision. We expect to see ~15 hits per event in the lead glass.

3.2. The High Resolution Streamer Chamber

A block diagram of the streamer chamber is shown in 3-2 and a sketch of the chamber is shown in fig. 3-3. This chamber will use the techniques of holographic photography and diffusion suprresion via negative ion storage of the ionization electrons during the trigger delay. The development work upon which our design is based is discussed in detail in Appendix III.

Table 3-3 summarizes the physical characteristics of the chamber and Table 3-4 summarizes its anticipated performance.

An interesting feature of this chamber is that the streamer density can be varied by changing the intensity of the photoionizing laser without

Table 3-3: Characteristics of the high resolution streamer chamber.

chamber volume	15 x 5 x 2 cm^3
sensitive volume (illuminated by photoionization laser)	15 x5 x 1.5 cm^3
distance between beam windows	~30 cm
operating pressure	60 atm
operating gas	90% Ne, 10% He .1% - .3% O_2, ~10 $\mu m CO_2$
radiation length	~650 cm
interaction length	~2.9×10^3 cm
photoionizing laser	
wavelength	351 nm
pulse length	~10 ns
energy per pulse	.5 to 1 Joule
high voltage pulse	
magnitude	≤500 kv
duration	~3 ns
timing jitter between high voltage and photoionizing laser	5 ns
delay between trigger and high voltage pulse	~1 μs

changing any other operating parameter of the chamber. Thus it will be possible to operate the chamber at the optimum streamer density such that the tracks are well defined yet the density is low enough that overlapping tracks can be recognized as such.

Table 3-4: Expected performance of the high resolution streamer chamber

streamer diameter	~20 μm
two track resolution	30μm
number of streamers/mm	~20
point setting error (σ) (projected view x depth view)	5 μm x 25μm
memory time (adjustable)	3-12 μs
dead time between pictures	0.1 sec

Another important feature of the design of the chamber system, motivated by our experience in E630, is its highly modular construction. Besides its advantages in the design and construction phases, the modular design will greatly increase the reliability and ease of maintenance of the system. We are paying particular attention to reliability in the design of the active components of the system. We plan to obtain the two lasers, the Marx generator, the gas system and the camera from commercial vendors who can supply well engineered and fully tested units. Suitable vendors for all these except the camera have been found. Given the CERN experience with the small high resolution bubble chambers, we are confident that the camera will not be a problem.

We are currently building the Blumlein section, the pressure barrier, the coaxial to parallel transmission line transition piece, the chamber module, the terminator and the gas system. Using our existing Marx generator, a camera from E630, and the excimer pumped dye laser from the development program for the holography laser and purchasing one additional laser for

photoionization, we will be able to operate the new streamer chamber with both holography and diffusion suppression. Because of the limitations of the existing Marx generator, optics, and camera, the sensitive volume in this test will be only 2 x 1 x 1 cm^3. However the chamber will operate at the full 60 atmospheres and be capable of demonstrating the expected resolution and streamer density. We plan to have this system assembled by the summer of 1985 and study its performance with electrons from a Ru^{106} source. The system with the more powerful Marx generator, larger optics, and new camera can be ready by the summer of 1986.

Figure 3-2: Block Diagram of the High Resolution Streamer Chamber System

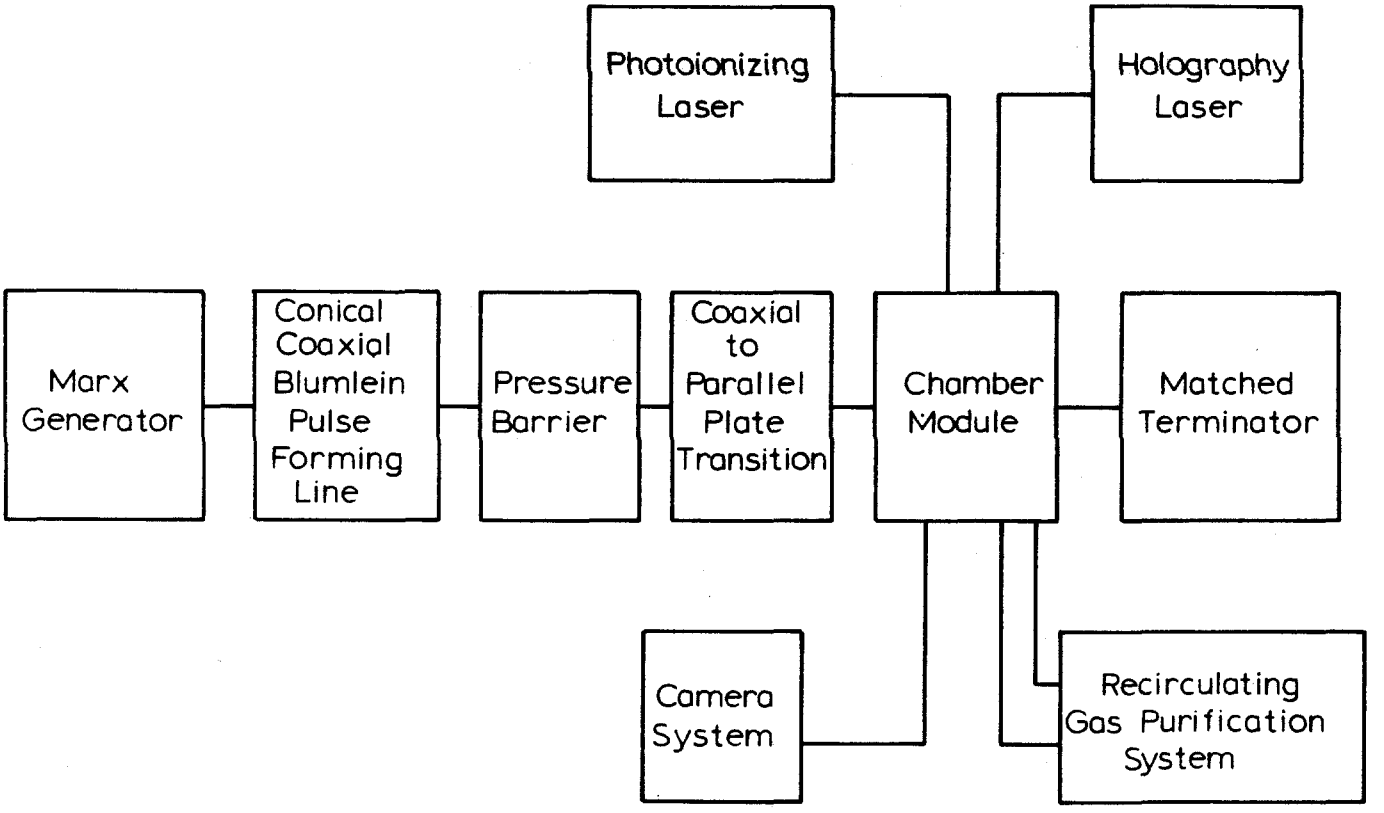

Figure 3-3: Sketch of the High Resolution Streamer Chamber

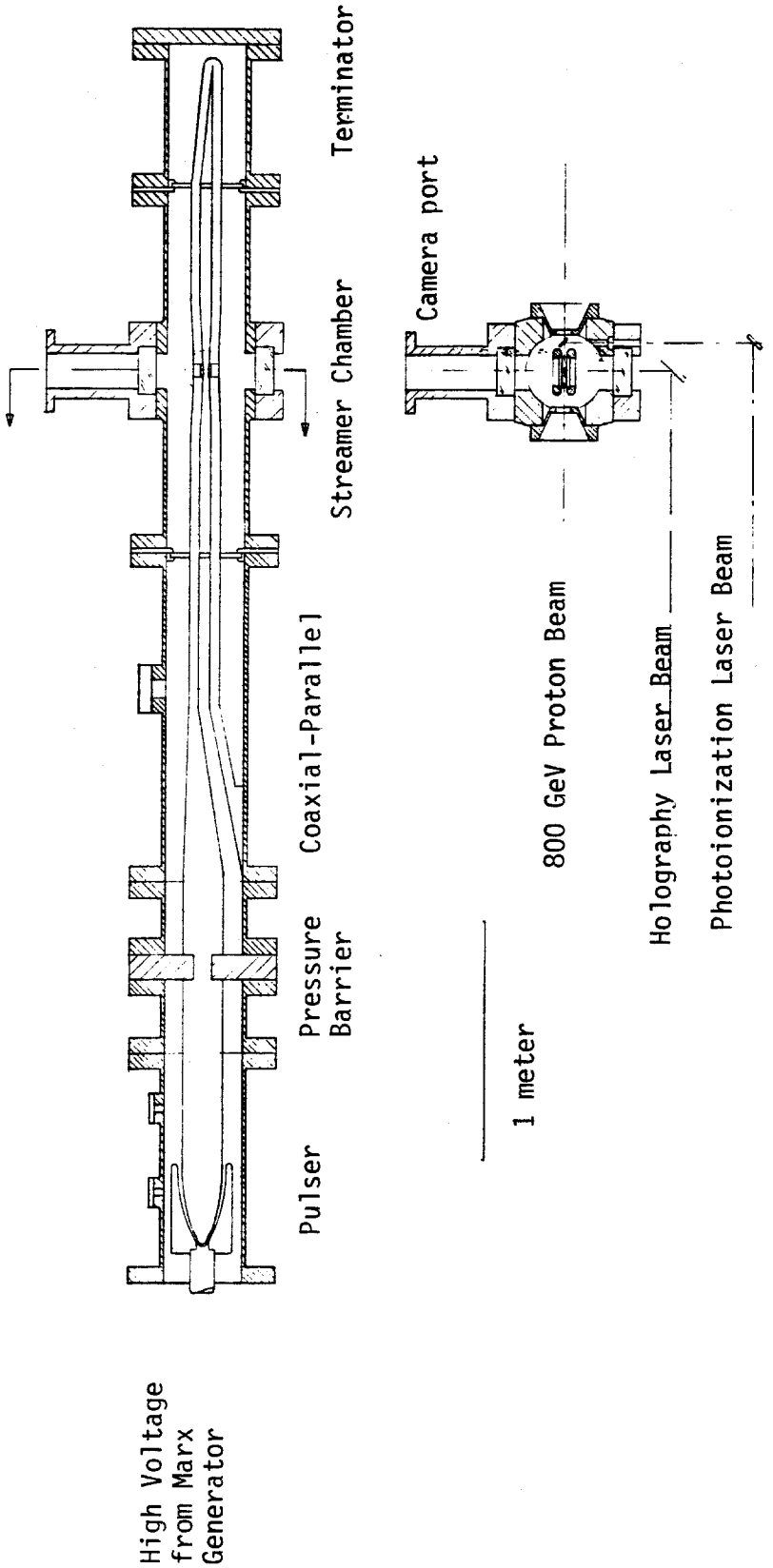

4. Event and Trigger Rates

In this section we:

1. present a calculation of the absolute event rate for the apparatus,

2. demonstrate, based on a Monte Carlo simulation, that the electron trigger discussed above with cuts in the fast processor of $P \geq 10$ GeV/c and $P_T \geq 1.2$ GeV/c reduces the trigger rate to an acceptable level,

3. present estimates of the signal to background ratios in the triggered sample.

4.1. Absolute Rate

The input to a calculation of the absolute event rate is:

1. σ - the pp cross section at 800 Gev; We use the inelastic value of 34mb. No triggers are expected from elastic scatters as the forward proton will pass through the beam hole and the backward one will seldom have enough momentum to reach the trigger apparatus.

2. α - the exponent in the atomic number dependence of the nuclear cross section, taken to be 2/3. This dependence is thought to be correct for the majority of the inelastic cross section. A stronger A dependance for heavy quark production will lead to somewhat better signal to background ratios but will affect the raw event rate negligibly and the trigger rate minimally.

3. ρ - the density of the target. The streamer chamber operating pressure is 60 atm; the gas is predominantly a mixture of 90% Ne, 10% He (by partial pressure or number of atoms).

4. L - the effective length of the fiducial volume for interactions; the value taken is 15 cm. The fiducial volume trigger will attempt to limit interactions to a desired region of length 10 cm, but it is assumed that due to finite resolution effects this longer region is more realistic.

5. I_{beam} - Average beam rate of 1.5×10^6 protons/sec.

Thermodynamics leads to an area density of 2.20×10^{26} nuclei/m^2, or .022 nuclei /barn. The mean inelastic cross section per nucleus is 235.6 mb for the chamber gas. Thus the fraction of (inelastically) interacting beam protons is .022 nuclei/barn x .2356 barns of cross-section/nucleus =

$\sim .18 \times 10^{-3}$

Combining factors yields an interaction rate of 7770/sec. As the deadtime of the streamer chamber is ~0.1 sec, the trigger must reduce the raw rate from 7770 Hz to at most a few Hz to avoid either considerable dead time losses or the loss of heavy quark events through a decreased beam rate.

4.2. Trigger Rates

In this section we discuss various sources of trigger particles - both from heavy quark decay and from background processes. We present expected trigger rates calculated by Monte Carlo techniques. The backgrounds considered are of three types:

1. Hadrons decaying directly to electrons.
2. Hadrons decaying to photons, followed by photon conversion to electrons.
3. Hadrons striking the TRD which are misinterpreted as electrons.

The basic procedure of the Monte Carlo program is the same for both signal and background events:

1. Electrons are generated with appropriate kinematic distributions (given below).
2. Particle paths are traced through the apparatus to see that they pass through the magnet aperture and strike three planes of TRD, without passing through the deadened central region of that device. The magnetic field is taken to be uniform between the pole faces. Vertical focussing due to non-normal passage of particles through the fringe field is also taken account.
3. The longitudinal and transverse momentum values are calculated using the algorithm of the trigger processor. This simulation includes resolution effects at the primary vertex and in the TRD, and the effect of the approximations made in deriving the formulas used in the processor. A particle is considered as leading to a trigger if its calculated momentum is within the

range 10-100 GeV/c and its calculated transverse momentum is greater than some particular value. Although the P_T cutoff is intended to be ~1.0 GeV/c, results are presented as a function of this parameter. This is done so that the effect of changing the P_T cutoff can be seen, and so that for cases where production processes make few high P_T particles, reasonable results can be obtained by extrapolation.

4. Normalization factors involving production cross sections, branching ratios, and TRD efficiencies are applied. All rates are calculated as a fraction of the inelastic cross section.

The processes studied are:

1. Experimental Signal $B \rightarrow e^{\pm} X$

We have assumed a production cross section for $B\bar{B}$ pairs of 50nb. This value is approximately the upper limit determined for hadroproduction of B's in experiments at lower energy. The model assumes central production of a $B\bar{B}$ pair parameterized, as was found for charm in hadronic collisions [8] by

$$\frac{d^3N}{dM\ dx\ dP_T} = \frac{1}{M^3} P_T\ e^{-cP_T} \cdot (1-|x|)^n \cdot e^{-d \cdot M/\sqrt{s}}$$

where M, x, and P_T refer to the $B\bar{B}$ pair, $c=2.2(GeV/c)^{-1}$, $n=3$, and $d=15$. The individual B mesons result from isotropic decay of the pair in its own rest frame.

The spectrum of electrons from B decays has been measured at CESR by running at the T(4S) [9]; that spectrum is reproduced here as Figure 4-1. The branching fraction to electrons has been measured in the same experiment and is given as $0.127 \pm 0.017 \pm 0.013$. The trigger rate for this process, and all others except a hadron faking an electron in the TRD, includes a factor of .729 - the efficiency for all three TRD modules firing on the passage of a legitimate electron.

Trigger rates per inelastic event as a function of P_T are given in Table 4-2 and shown in summary in Figure 4-4.

2. Experimental Signal $D \rightarrow e^{\pm} X$

The calculation of charm trigger rates is similar to that for B's. The assumptions used are:

a. The $D\bar{D}$ cross section is taken to be 50μb.

b. The production dynamics follows the same form as given for

B's with parameters c=1.3 $(GeV/c)^{-1}$, n=6, and d=20.

c. Charged and neutral D's are produced in equal numbers.

d. Branching fraction for $D^{\pm}$ $\rightarrow e^{\pm}X$ is 0.17±.03±.03, for $D^{o}/\bar{D}^{o} \rightarrow e^{\pm}X$ is 0.06±.02±.02 [4]. The spectrum of electrons from D decay is as measured by DELCO [10] and reproduced here as Figure 4-2.

The results of the acceptance calculation are given in Table 4-2 and shown in summary Figure 4-4.

3. Background Processes

4. The background processes considered all involve either the daughter particles of π, K, η, or vector mesons or the misidentification of charged π's or K's themselves. The production model for these light hadrons is taken from ISR results [11]. The rapidity and transverse momentum distributions for pions and kaons result from a parameterization of Figure 24 and Figure 25 of ref. [11]. These figures are reproduced here as numbers 4-3a and 4-3b. The vector and η mesons are assumed to have the same distribution as the pions. These ISR data represent measurements taken near 90° in the c.m. and are a measurement of the central production process, the source of the great majority of produced hadrons. Diffractive dissociation of the incident proton has also been considered. However the cross section for this process at 800 GeV/c is low enough and the P_T distributions narrow enough that contributions are small compared with those from centrally produced hadrons.

4.3. Background Processes

4.3.1. Direct Decay to Electrons

The decays considered and appropriate normalizing factors are listed in Table 4-3. For the neutral particle decays (except K^o) listed the electrons are emitted essentially from the production point. Thus the trigger processor algorithm yields, except for resolution effects, the true longitudinal and transverse momenta. However for the charged particles (and K^o's), which have much longer mean lifetimes, the electrons are in general not emitted from the production point and the algorithm values can differ substantially from the actual ones. In our calculations this effect

has been considered, including the effects of decays before, inside, and after the magnetic field region. It should be noted that electrons with actual momenta of less than 1.0 GeV/c will not be detected with any reasonable efficiency in the TRD (Lorentz γ is too low) and are thus not considered.

Trigger rates for the above processes are given in Table 4-4.

4.3.2. Decay of Hadrons to photons, followed by conversion to electrons

The decays considered here together with appropriate normalization factors are given in Table 4-5.

A careful study has been made of the various materials in the detector which can lead to conversions. Table 4-6 lists those used in the calculation.

All conversions are generated with both electrons of the pair maintaining the original direction of the photon with the only direction changes coming from the magnetic field. The energy distribution of the electrons is uniformly distributed from zero to the total photon value. The result of these assumptions is that for conversions before the magnet the electrons behave in the same manner as do those produced at the interaction point. However for conversions occurring after the magnet the electrons in the TRD point directly at the target and would be given an infinite momentum by the trigger processor were it not for resolution effects. These effects actually lead to calculated values of $P \geq 100$ GeV/c with a peak at ~250 GeV/c. To reduce this source of background triggers we impose a cut of 100 GeV/c maximum electron momentum. For those occasional electrons

which, due to resolution effects different in practice from those used in our simulation, are calculated to have momentum less than 100 GeV/c, the requirement that the energy measured in the appropriate lead glass blocks be equal to the momentum calculated in the TRD (within errors) leads to an effective trigger suppression.

Due to the large flux of photons from the target a non-negligible number of conversions can occur in the helium in the region of the magnetic field. Those $e^{\pm}$ from conversions near the upstream end behave similarly to electrons from the target, those near the downstream end similarly to $e^{\pm}$ from conversions beyond the field. Then there is a long region representing a smooth transition between these extremes. Electrons produced here pass through some magnetic field but not so much as assumed in the processor algorithm. Thus they have a calculated longitudinal momentum much higher than the actual value but not necessarily greater than the 100 GeV/c cutoff. The calculated P_T is also much higher than the actual value. In our simulation such electrons (for P_T calculated as greater than 1.0 GeV/c) never have an energy as seen in the lead glass of even 80% of the calculated momentum in the TRD. These electrons can lead to triggers only if overlap of photons or hadrons in the lead glass supply enough energy to satisfy the energy-momentum comparison in the processor. This overlap problem has been studied in detail for the case of hadrons faking electrons in the TRD and is discussed below. In summary, the conversions in (and after) the magnet are not nearly so serious as are those before it. The results of this section are summarized in Table 4-7.

4.3.3. Charged hadrons faking electrons in TRD

There are a large number of charged hadrons, $\pi^{\pm}$ and $K^{\pm}$, from normal central production events which pass through the TRD. The detection efficiency for them as electrons is 13% per module or 2.2×10^{-3} for the three modules used in the trigger. In addition to hadrons directly counting in the PWC's of the TRD, it is also possible for hadrons to interact in the TRD modules in such a way as to look like an electron track. An analysis shows that this process effectively doubles the rate of hadrons faking electrons in the TRD. Single particle π and K production has been simulated with these particles treated as if they were target produced electrons but with the efficiency factor given. This effect yields a trigger rate from the TRD alone for π's (K's) of 3.30×10^{-4} (4.6×10^{-5}) per inelastic event, or a total rate of 3.76×10^{-4}, for a P_T cut of 1.0 GeV/c. Thus, these hadrons represent a background about equal to that of the processes discussed above. While not the dominating effect in trigger rate calculations, they would cause serious problems later in the analysis if not suppressed. As is discussed elsewhere in this proposal, many of the background events containing legitimate electrons, and in particular those containing electrons from conversions, can be eliminated by off-line analysis either prior to looking at the streamer chamber hologram, or after looking at it but prior to complete measurement. Similar techniques will not work for these fake electrons, so that holograms would have be measured before these events can be eliminated. In this case the hadron background would represent a large fraction of the measurement load if not eliminated.

Most of this backgound can be eliminated by comparing the energy

deposited in the relevent lead glass blocks with the TRD momentum of the assumed electron. For true electrons the two values will be the same to within errors, while for hadrons the energy from the shower will in general be much less. If a cut is imposed that the shower energy be at least 80% of the TRD momentum value, and with the possibility of studying the longitudinal shower development, it is assumed based on prior experience that the hadron background can be reduced to negligible proportions.

While the above analysis is correct for particles generated and studied one at a time, there are complications due to many-particle effects in complete events. A way in which the lead glass can fail to eliminate a hadron faking an electron is if other particles of the event, in particular photons from π^o and η^o decay, supply enough energy to make it comparable to the TRD momentum. To study this effect the individual hadrons which have produced background triggers in the Monte Carlo simulation have been made elements of typical central production events. Such events are generated by assuming Poisson distributions for the numbers of charged pion pairs, π^o's, and η^o's and using our single particle production model for all particles except the triggering hadron. Although this procedure conserves charge, no attempt is made to conserve energy, momentum, or strangeness. The π^o's and η^o's decay the proper fraction of the time via the $\gamma\gamma$ mode and all of the produced hadrons and photons are extrapolated to the upstream surface of the lead glass. All photons are assumed to deposit 100% of their energy in the glass at this spot, all hadrons 10%. An area surrounding the trigger hadron is now examined to see how much energy is deposited therein. The area selected is that occupied by four 15 cm x 15 cm cross section blocks, the largest area likely to be included by the

processor. If one now considers as triggers any hadrons for which there is energy of at least 80%·P in the appropriate region, 11.8% of the original sample remain, leaving a hadronic (fake electron) trigger rate of 4.44×10^{-5} per inelastic event.

As noted, this 11.8% effect of the 'overlap' problem is for a P_T cut of 1.0 GeV/c. This fraction will differ for other cut values since the distributions in position of lead glass hits for these particles is a function of their mean P_T. (At lower P_T the particle density in the lead glass increases.) However this value is still expected to yield the proper order of magnitude for other P_T values and is assumed in the data presented to be independent of the cutoff value. The results are given in Table 4-8.

The results of this section are summarized in Figure 4-4.

4.4. Summary

In the first part of this section the total inelastic event rate has been calculated to be ~7770 Hz. In the second part the various sources of triggers, for a P_T cutoff of 1.2 GeV/c, yield a fraction of the inelastic events totaling 2.1×10^{-4}. Thus a raw trigger rate of 1.6Hz and a gated trigger rate of 1.4Hz is indicated. The 16% dead time for an assumed 10 Hz system seems acceptable. For the values given the charm sample represents 4.4% of the triggers, the B's .03%, enhancements by factors of 30 and 218 respectively over the raw event rates. Of these heavy quark triggers, 67% will be for measurable events in the streamer chamber fiducial volume.

Our request for beam time and a summary of the various rates is given in table 4-1 below.

Table 4-1: Summary of Beam and Event Rates

Hours requested	1000
Assumed Accelerator Duty Cycle	1/3
Beam	800GeV/c protons
Instantaneous Beam Flux	1.5MHz
Raw Interaction Rate in 15cm of Chamber Gas	7.77KHz
Ungated Trigger Rate	1.6Hz
Gated Trigger Rate	1.4Hz
Total Number of Holograms Taken	1.63×10^6
Number of Holograms with Interaction in 10cm Fiducial Volume	1.09×10^6
Number of Fiducial Interactions with $B\bar{B}$ (50nb production cross section assumed)	350
Number of Fiducial Interactions with $D\bar{D}$ (50μb production cross section assumed)	4.86×10^4
Enhancement of $B\bar{B}$ in Triggered Pictures Relative to Raw Interactions	218
Enhancement of $D\bar{D}$ in Triggered Pictures Relative to Raw Interactions	30

Table 4-2: Trigger rates per inelastic event for B and D production as a funtion of P_T.

p_T cutoff (GeV/c)	.5	1.0	1.5	2.0
B-->e	1.03×10^{-7}	8.02×10^{-8}	4.65×10^{-8}	2.19×10^{-8}
D-->e	5.02×10^{-5}	1.54×10^{-5}	4.40×10^{-6}	1.28×10^{-6}

Table 4-3: The decays and appropriate normalization factors for the background from direct decay of hadrons to electrons.

Decaying Hadron	#/Inelastic Evt	Mode	Branching Fraction
π^o	5.2	γe^+e^-	1.15×10^{-2}
$\pi^\pm$	10.4	$e^\pm\nu$	1.267×10^{-4}
		$e^\pm\nu\pi^o$	1.02×10^{-8}
$K^\pm$	.56	$e^\pm\nu$	1.54×10^{-5}
		$e^\pm\nu\pi^o$	4.82×10^{-2}
η^o	2.6	γe^+e^-	5.0×10^{-3}
ρ^o	0.3	e^+e^-	4.3×10^{-5}
ω^o	1.0	e^+e^-	7.6×10^{-5}
ϕ^o	0.1	e^+e^-	3.1×10^{-4}
K^o	0.28	$\pi^o\pi^o$ (one π^o-->$e^+e^-\gamma$ and one π^o-->$\gamma\gamma$)	7.53×10^{-3}

Table 4-4: Background trigger rates as a function of P_T due to the direct decay processes of table 4-3.

p_T cutoff (GeV/c)	.5	.75	1.0
Mode			
$\pi^o \rightarrow \gamma e^+ e^-$	4.55×10^{-4}	1.48×10^{-4}	4.36×10^{-5}
$\pi^\pm \rightarrow e^\pm \nu$	2.08×10^{-7}	7.12×10^{-8}	2.37×10^{-8}
$\pi^\pm \rightarrow e^\pm \nu \pi^o$	negilible		
$K^\pm \rightarrow e^\pm \nu$	1.75×10^{-8}	7.76×10^{-9}	3.11×10^{-9}
$K^\pm \rightarrow e^\pm \nu \pi^o$	$\sim 1 \times 10^{-7}$	$\sim 1 \times 10^{-7}$	$\sim 1 \times 10^{-7}$
$\eta^o \rightarrow \gamma e^+ e^-$	1.50×10^{-4}	2.97×10^{-5}	8.82×10^{-6}
$\rho^o \rightarrow e^+ e^-$	1.01×10^{-6}	1.98×10^{-7}	4.61×10^{-8}
$\omega^o \rightarrow e^+ e^-$	6.34×10^{-6}	1.36×10^{-6}	3.43×10^{-7}
$\phi^o \rightarrow e^+ e^-$	4.80×10^{-6}	8.60×10^{-7}	1.97×10^{-7}
$K^o \rightarrow \pi^o \pi^o$ + Dalitz	2.29×10^{-5}	5.13×10^{-6}	2.11×10^{-6}

Table 4-5: Decays contributing to background by hadron decay to photons followed by photon conversion.

Decaying Hadron	#/Inelastic evt	Mode	Branching Fraction
π^o	5.2	$\gamma\gamma$	.9885
η^o	2.6	$\gamma\gamma$	.38
K_s^o	0.28	$\pi^o\pi^o$ both $\pi^o \rightarrow \gamma\gamma$	.3067
ρ^o	0.3	$\pi^o\gamma$	2.4×10^{-4}
ω^o	1.0	$\pi^o\gamma$	8.8×10^{-2}
ϕ^o	0.1	$\pi^o\gamma$	1.4×10^{-3}

Table 4-6: List of materials in the apparatus used to calculate photon conversions.

Material	Comment	Rad L (cm)	Conversion Probability per γ
Streamer chamber gas 90% Ne, 10% He 16.5cm on average	60 atm	650.0	2.53% (average)
exit window	0.125mm Fe	1.76	.72%
electrode*	glass	12.7	----
electrode holder*	brass	1.43	----
Air before magnet	192.5 cm	30423.	.63%
Air after magnet	300 cm	30423.	.99%
PWC's before magnet 3 stations 3 planes each	---	----	.30%
PWC's after magnet 3 stations 3 planes each	---	----	.30%
Helium in magnet	350 cm	582294.	.060%

(*) The streamer chamber electrodes and electrode holders are situated beside and close to the interaction region. They are traversed by wide angle photons with a length of material dependent on angle and interaction point.

Table 4-7: Trigger rates as a function of P_T due to the process of table 4-5.

p_T cutoff (Gev/c)	.50	.75	1.0
Mode			
$\pi^o \rightarrow \gamma\gamma$	2.43×10^{-3}	6.67×10^{-4}	2.73×10^{-4}
$\eta^o \rightarrow \gamma\gamma$	7.28×10^{-4}	1.43×10^{-4}	4.25×10^{-5}
$K^o \rightarrow \pi^o \pi^o$ (both $\pi^o \rightarrow \gamma\gamma$)	5.70×10^{-5}	4.61×10^{-5}	3.86×10^{-5}
$\rho^o \rightarrow \pi^o \gamma$	3.97×10^{-8}	8.24×10^{-9}	1.52×10^{-9}
$\omega^o \rightarrow \pi^o \gamma$	4.79×10^{-5}	8.16×10^{-6}	2.57×10^{-7}
$\phi^o \rightarrow \pi^o \gamma$	1.55×10^{-7}	2.80×10^{-8}	3.16×10^{-9}

Table 4-8: Trigger rates as a function of P_T for hadrons faking electrons in the TRD.

p_T cutoff (GeV/c)	.5	1.0	1.5	2.0
Hadrons faking electrons	3.74×10^{-4}	4.44×10^{-5}	7.04×10^{-6}	6.18×10^{-7}

Figure 4-1: Measured spectrum of the electron in the B rest frame.

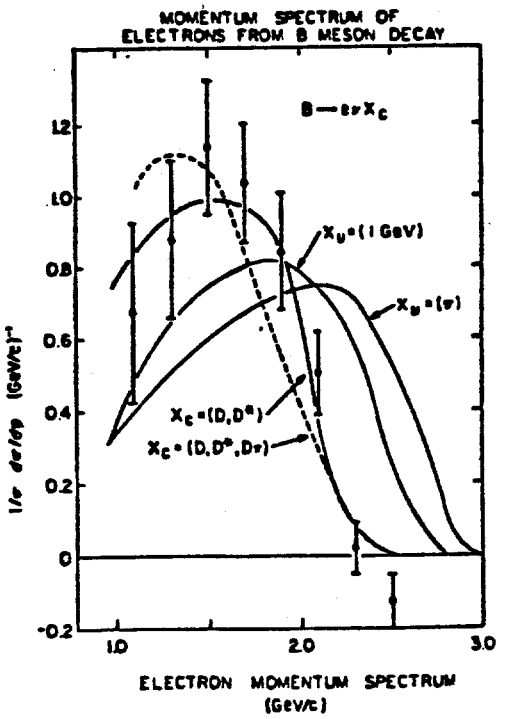

Electron momentum spectrum from B decays.

Figure 4-2: Measured spectrum of the electron in the D rest frame.

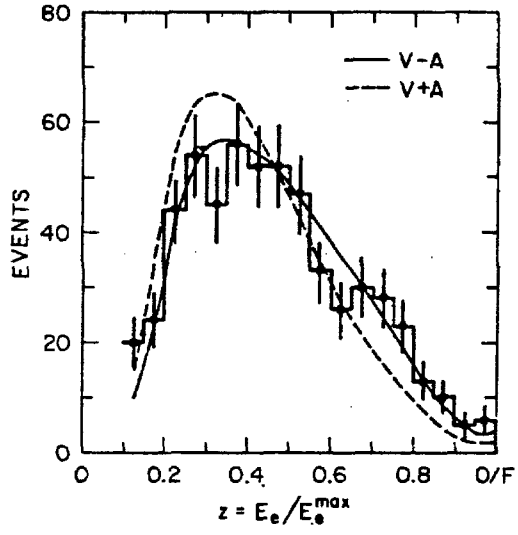

The electron momentum spectrum expressed as $z = E_e/E_e^{max}$, in the range $3.57 \leq E_{c.m.} \leq 7.4$ GeV, excluding data taken at the $\psi''(3770)$. The solid and dashed lines are, respectively, $V-A$ and $V+A$ fits with zero ν_τ mass.

Figure 4-3: Inclusive single particle distribution in rapidity and transverse momentum for $\pi^{\pm}$ (a.) and $K^{\pm}$ (b.).

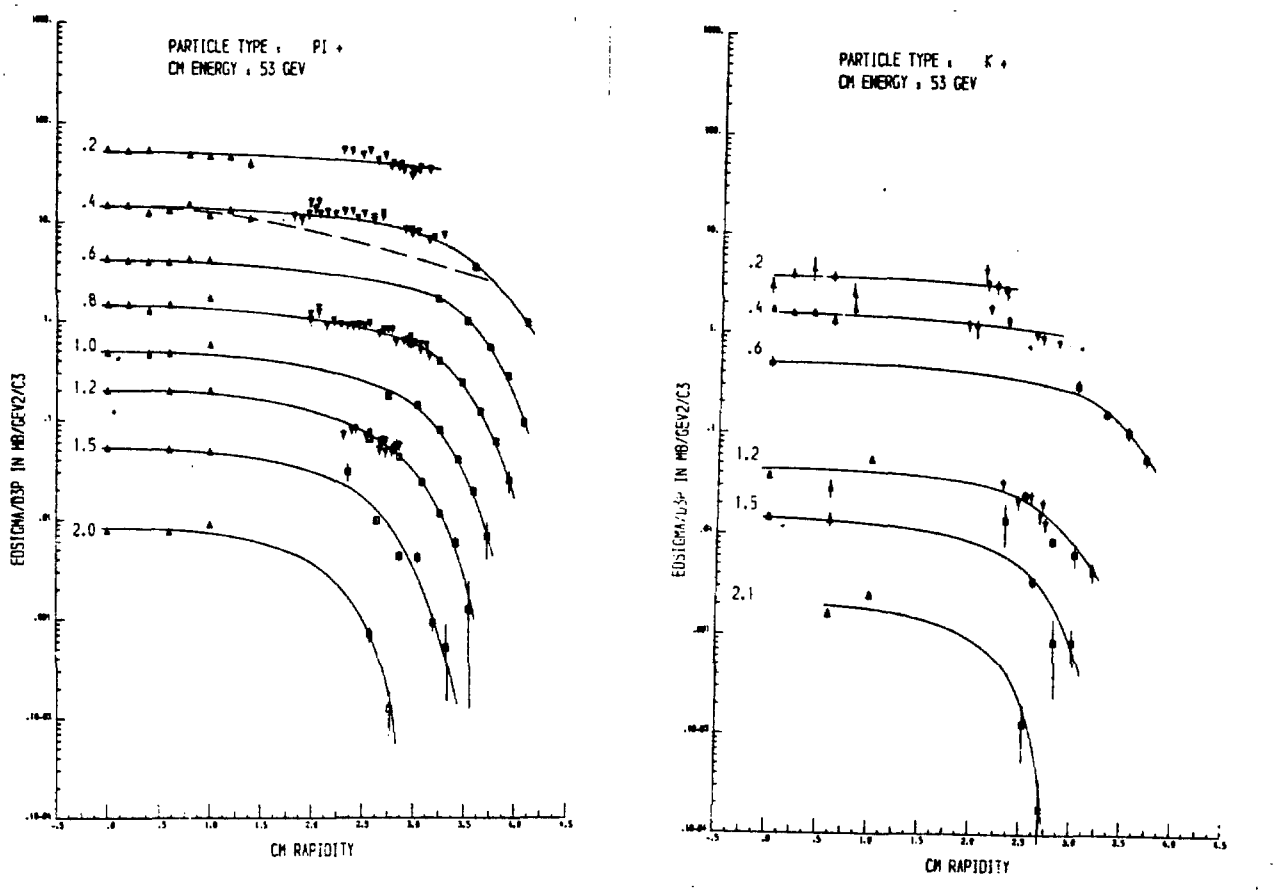

The invariant cross section for production of π^+, K^+ as a function of p_T and y, at $\sqrt{s}$ = 53 GeV. Δ: Points from this experiment; □: measurements by the CERN-Holland-Lancaster-Manchester Collaboration; ∇: measurements by the CERN-CEN-Bologna Collaboration. Handdrawn curves have been made to indicate the points measured at the same value of p_T. For π^+ and p_T = 0.4 GeV/c the dashed line shows the continuation of the Gaussian fitted to the data at small y out to large y.

Figure 4-4: Trigger rates expressed as fraction of inelastic events for various signal and background processes. The rates are presented as a function of the P_T cutoff to be applied.

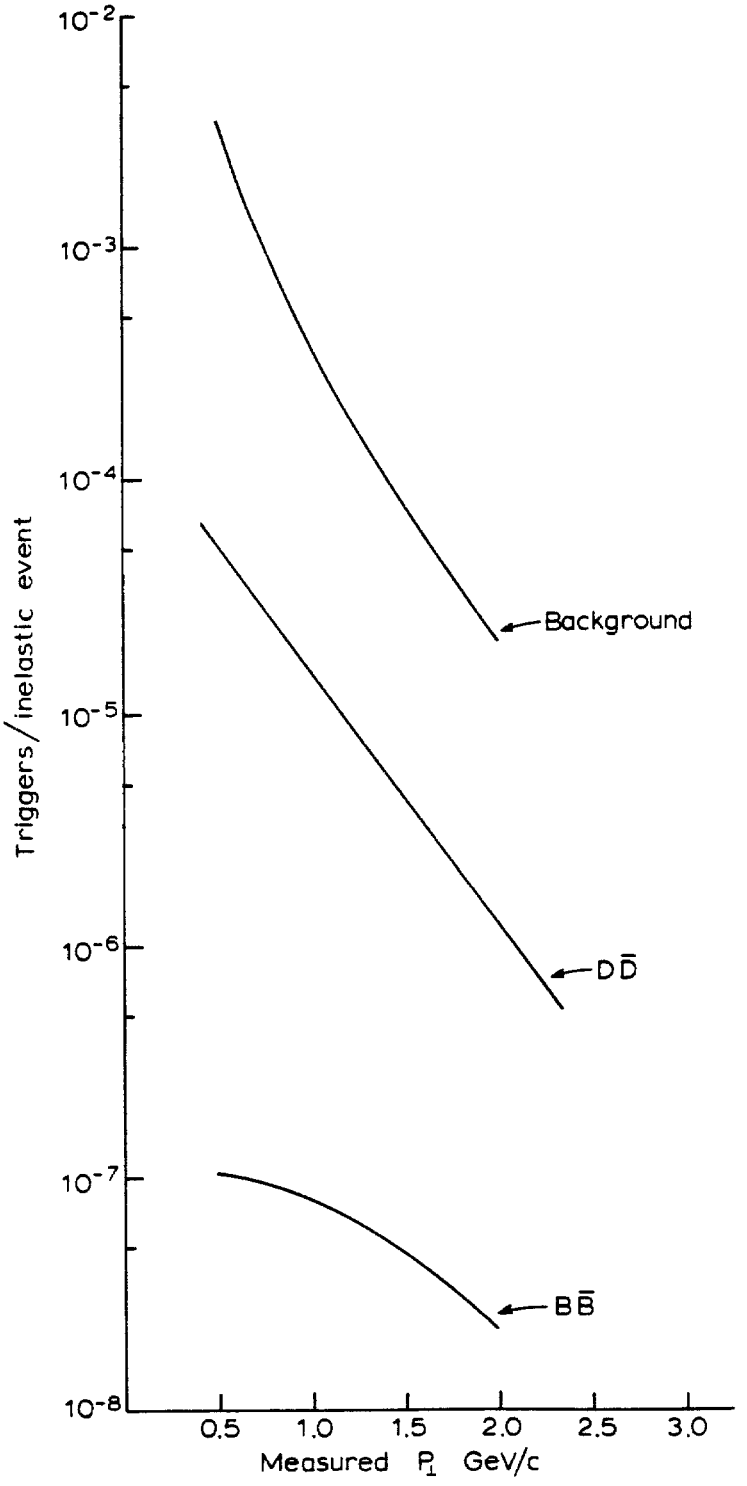

5. Data Analysis

This section discusses the logistics of the analysis and describes the procedures we are developing to identify the beauty and charm events in the trigger sample.

5.1. Logistics

We recall that we expect to record 1.63×10^6 holograms of which 1.09×10^6 contain interactions in the fiducial region.

The first step in the procedure is the off line analysis of the downstream spectrometer data to produce a selected list of events to measure. The off line cuts will effectively improve the trigger via the following steps:

1. The selection of the trigger processor is checked using a sharpened measurement of P and P_T and a more sophisticated analysis of the lead glass data.

2. A large fraction of the fake triggers due to conversion electrons can be removed by checking for the electron track in the PWC's upstream of the magnet and, most importantly, by searching for the other electron or positron in the conversion. Monte Carlo studies indicate that 2/3 of the fake triggers can be eliminated in this way.

The restricted scan list will then contain 5.44×10^5 pictures containg 3.63×10^5 fiducial interactions. We expect, as was noted in the section on rates, that this sample will contains 4.86×10^4 charm events or about 1 charm event in every 7.5 fiducial pictures.

We plan to futher reduce this sample by a quick measurement aimed at identifying the trigger electron in the picture. Using the PWC nformation, the computer controlled projection system locates the beam

track. The measurer then follows the beam track to the interaction point which is then recorded. (Non-fiducial or inconsistent interactions are quickly discarded.)

The measured vertex and the angle of the trigger electron track as measured in the spectrometer are used to define a road or "error cone"in the picture for the electron track. If no track is consistent with this road the event is discarded. If there is a track in the road, a few points are measured and the computed angle is checked against the spectrometer angle. If the event passes, a careful measurement is made of the complete event.

We estimate that this process will reduce the sample which requires careful and time consuming measurement to ~100,000 events with a charm content of 50% and with a $B\bar{B}$ event every 280 pictures.

We emphasize that our approach does not involve detecting heavy quark decays by scanning. Instead, we use measurements on each viable candidate. This procedure, which eliminates scanning biases is only possible because of the triggerability of the streamer chamber and the synergistic use of the data from the downstream apparatus. We note that in E630 [12], [13] exactly this strategy of using the off line analysis allowed us to reduce the sample of 20138 triggered fiducial interactions (which already had a charm enhancement of about 55 from the trigger requirements) to a sample of 1807 pictures to be measured.

The experience decribed in the appendix on hologram analysis indicates

that ~5,000 holograms per shift per year can be measured on a machine of the Brussels type. In the collaboration we expect to have 4 machines running 2 shifts a day corresponding to a measuring capacity of 40,000 holograms per year. Thus the complete measurement job can be completed in ~2.5 years.

We note, however, that using the offline analysis we can selectively analyze particular data samples early. This can be done to produce early samples of beauty events (by increasing the P_T cut), multi-electron events for $\Gamma(D^o \rightarrow e x \nu) = \Gamma(D^+ \rightarrow e x \nu)$ test, and F meson studies using the $\phi\pi$ decay mode.

5.2. Identification of Beauty and Charm

Next we will discuss the identification of beauty and charm in the events which have survived the selection described above and which have been carefully measured. Table 5-1 lists the expected properties of the measurements in the streamer chamber pictures.

The method of analysis which we discuss here has evolved, in part, out of our experience with E-490 and E-630 and in part from an on-going program of Monte Carlo simulations.

A Monte Carlo simulation program [14] has been written which generates events, both $B\bar{B}$ and $D\bar{D}$ production, according to production models very similar to those described in the section on rates. This program generates complete events including the hadrons produced in association with the $B\bar{B}$ r $D\bar{D}$ systems. The B and D particles are tracked and allowed to decay using the best current estimates of the lifetimes and branching ratios. In

Table 5-1: Measurement Characteristics of Streamer Chamber Pictures

Two Track Resolution	30 μm (in space)
Point Setting Error for Track Measurement	5 μm (in space)
Fiducial Region	10 cm
Total Visible Region	15 cm
Streamer Density	15-20 streamers/mm (in space)

particular the lifetime of the B particles has been taken to be 10^{-12} sec.

The program then generates tracks in the streamer chamber and simulates the measurement process including resolution effects and blocking effects due to overlapping track sections. The measured points are then analyzed with track fitting programs, etc., just as would be done with measurement data. To date, we have only studied the X-Z projections of the measured and fitted tracks. (The X-Z plane is the plane of the streamer chamber window.) Thus our results are very conservative; work is underway to use the depth information which will improve the selectivity beyond that presented below.

We have also developed a plotting program to simulate the appearance of the projected picture (of the reconstructed hologram) on the scanning table. This program assumes 30μm diameter streamers with 15 streamers per mm. The streamer centers are assumed to have a Gaussian distribution

transverse to the track direction with a standard deviation of 10μm. The combination of these parameters produces tracks with a two track resolution of 30μm.

The analysis proceeds by first determining the position of the primary vertex. This is done from the measured position augmented by vertex fitting using the wide angle tracks whose projected angle with respect to the beam is ≥100mr. Then the "miss distance", S, and its error, DS, is calculated for each measured track.

For the detection of charm events the requirement that there be at least one track with $|S/DS| \geq 4.0$ is an efficient algorithm. We find that 93.4% of all charm production satisfies this requirement and less than 1% of the "ordinary" hadronic interactions satisfy it. In the case where the D^{o} decays into 4 charged particles, or the $D^{\pm}$ decays into 3 particles, it is almost always possible to properly verticize the decay point. In the case of 2 prong D^{o} decays or one prong $D^{\pm}$ decays, the projected data alone is not always adequate to reconstruct the vertex. However, it is possible to assign the decay tracks to the correct parent. For example, we will know that a D^{+} decayed into a single positive track but will not be able to uniquely determine the decay point.

We expect the use of the depth information will substantially improve this, especially for 2 prong D^{o} decays.

The identification of beauty production events is a more difficult task ecause of the large charm background. A careful analysis of the picture

and the data, by a physicist, is required to obtain the best results.

In order to provide a conservative estimate of the efficiency of unambiguously detecting beauty events we have developed an algorithm, which uses only the measured track data, to pre-select the events to be studied by a physicist. This algorithm is:

1. Require a least 1 track with $|S/DS| \geq 10.0$
2. Require at least 4 tracks with $|S/DS| \geq 5.0$
3. Require $\Sigma|S/DS| \geq 225.0$, where the sum is over all measured tracks in the event.

This algorithm is 56% efficient for beauty but only 4% efficient for charm. Since the charm to beauty ratio in our triggered pictures is expected to be ~140, the charm to beauty ratio in the events selected by the algorithm is expected to be ~10. A physicist analysis is then required to unambiguously detect the beauty events in this sample. We have generated events as noted above and selected them according to this algorithm. It appears that in essentially all the beauty events selected by this algorithm it is possible to ascertain that they cannot be charm events (identifying more than two decay veritces, finding a trigger electron which does not come from either of two identified decay vertices, etc.).

We repeat that we have not yet used any depth information in the chamber and we have not used any downstream data that would allow charge balancing studies, visible mass measurements, P_T measurements, etc. We thus conclude that we can identify beauty events with an efficiency of at least 50%.

We conclude this section with an illustration of how such an analysis would proceed in a typical beauty event. Figure 5-1 (fold-out) shows the simulated streamer chamber projection for the following reaction which passed the $B\bar{B}$ filter algorithm:

$$p + p \rightarrow B^0 + \bar{B}^0 + 7\pi^\pm + \text{neutrals}$$

$$B^0 \rightarrow D^+ + e^- + \bar{\nu}_e$$
$$D^+ \rightarrow K^- + \pi^+ + \pi^+ + \pi^0 + \pi^0$$

$$\bar{B}^0 \rightarrow \bar{D}^0 + \pi^+ + \pi^- + \pi^0$$
$$\bar{D}^0 \rightarrow K^+ + \pi^+ + \pi^- + \pi^- + \pi^0$$

This figure illustrates the very large information content in the streamer chamber pictures. All the tracks eventually separate and become ndividually measureable at various distances from the vertex. With 15-20 streamers/mm there is essentially one measurement with a σ of 5μm for every mm of track and each track can be measured over its maximum unobscured length.

Figure 5-2 shows this event in the streamer chamber. Figure 5-3 shows the event again, this time in an anamorphic perspective view such that the longitudianal magnification (along the beam direction) is different from the transverse magnification. Such plots [15] are very useful in the pattern recognition process. In this transformation the magnification also decreases with distance from the vertex and angles are magnified. The plot produces a view very similar to to what would be observed by placing one's eye at the edge of the scanning table and sighting down the event. Figure 5-4 shows the plot with all tracks except those due to the decaying

particles removed.

The next figure, 5-5, shows the measured tracks. All tracks have been projected back to the longitudinal coordinate of the primary vertex. The next step is to remove all tracks which have $|S/DS| \leq 3$ with respect to the primary vertex. The results are shown in figure 5-6. Here one sees a good 4 track vertex in the lower right hand section of the plot. The final plot, figure 5-7 shows the tracks remaining after the 4 tracks which make up the 4 track vertex have been removed. It is clear that the remaining tracks are not consistent with a single vertex. Indeed, a fit (in the X-Z projection) of these four tracks to the hypothesis of a single vertex gives a chi-squared of 73 for 2 degrees of freedom.

Thus this event cannot be described with 2 secondary verticies. In figure 5-7 both tracks from the $\overline{B}^{o}$ decay are missing because they had $|S/DS| \leq 3$. Knowing that the event is a $B\overline{B}$ event, the tracks can be re-examined and the cut on S/DS made less stringent. Using the downstream data (momenta and charge of the tracks) and requiring kinematic consistency with the decay tracks that have been clearly established using the more stringent S/DS cut, the remaining B^{o} decay tracks can be identified. In particlular, in this event, the two B decay tracks removed by the $S/DS \geq 3$ cut both have $S/DS > 3$. No track from the primary vertex in this event has $S/DS > 1.5$.

Figure 5-1: A computer simulated projection of the reconstructed hologram from a $B\bar{B}$ production event in the streamer chamber. The projection is 30 times life size. See text for the details of the event and the simulation.

[SEE FOLD-OUT ENCLOSED]

Figure 5-2: A projection of the selected $B\bar{B}$ *production event in the streamer chamber.* This picture is .83 times life size.

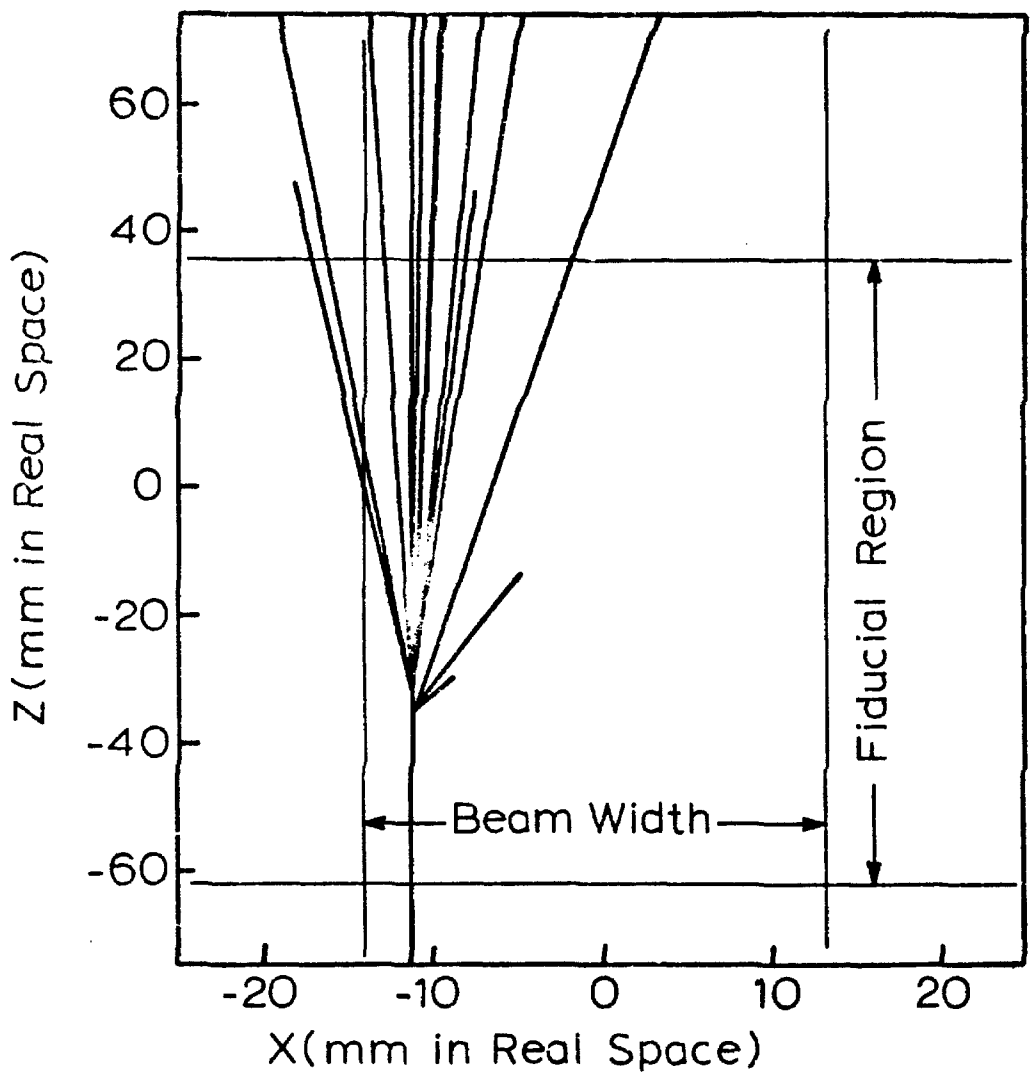

Figure 5-3: An anamorphic perspective view (Dreverman plot) of the selected $B\bar{B}$ event. The B and the D particle decays are now clearly visible.

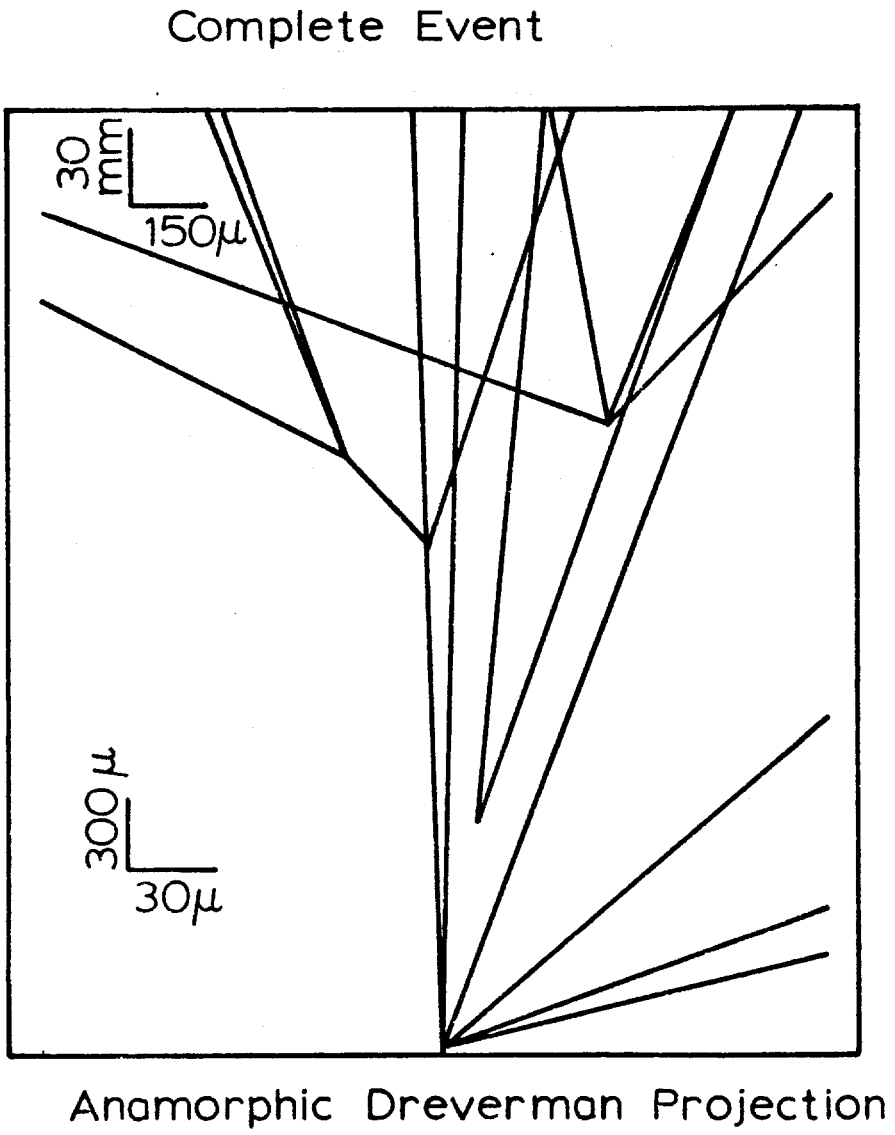

Figure 5-4: An anamorphic perspective view of the selected $B\bar{B}$ event showing only the particles that decay in the chamber.

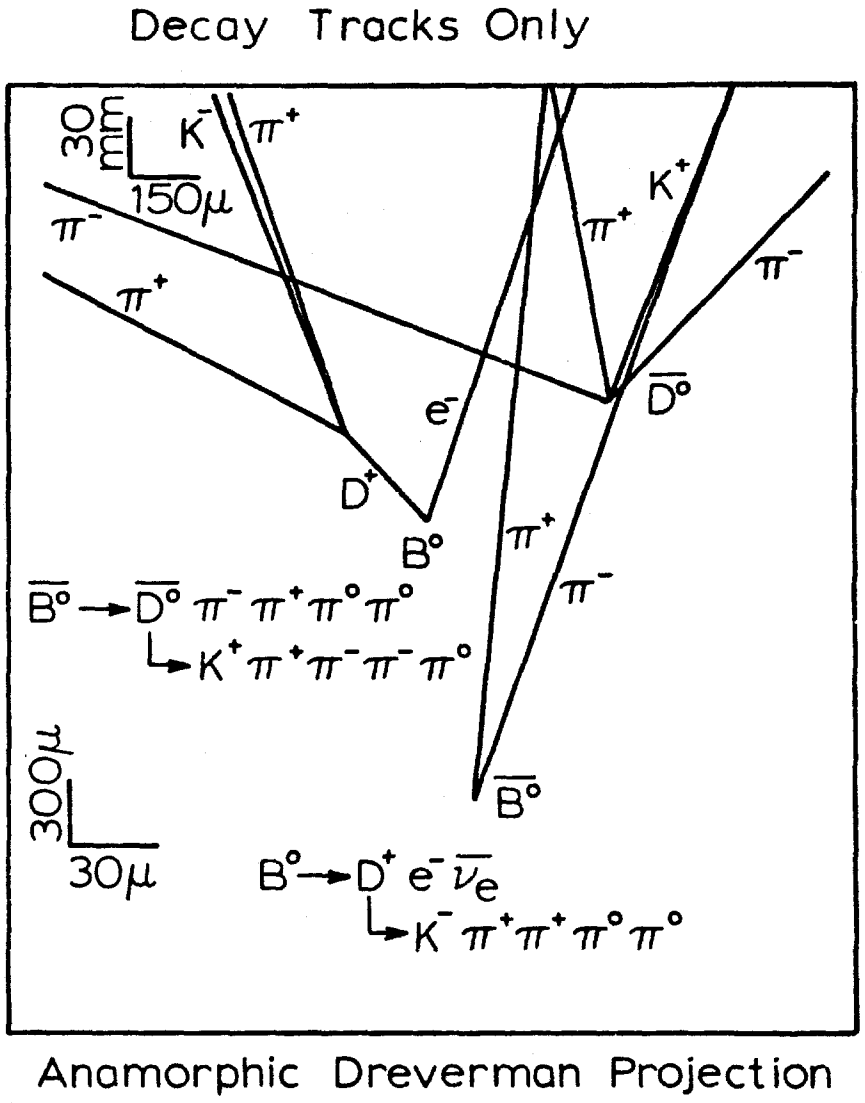

Figure 5-5: An anamorphic perspective plot of the measured tracks in the selected $B\bar{B}$ event.

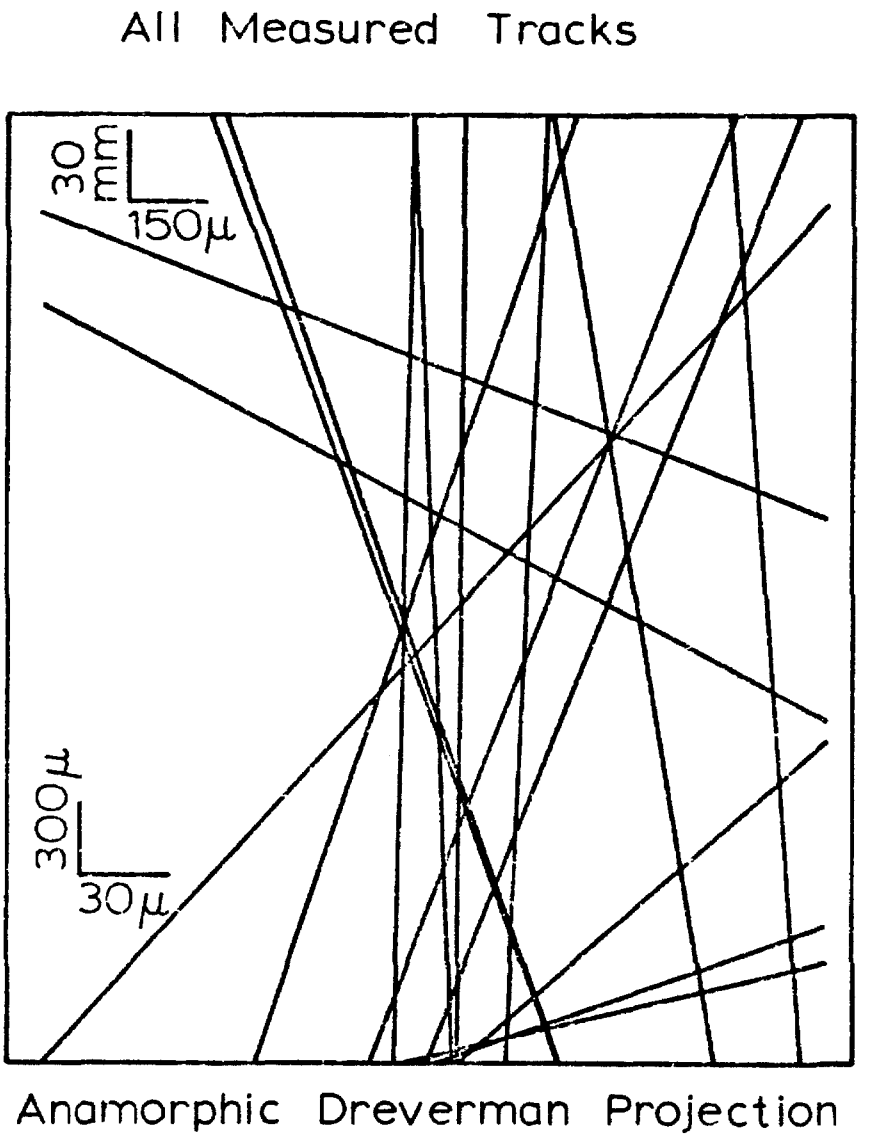

Figure 5-6: An anamorphic perspective plot of the measured tracks, in the selected $B\bar{B}$ event, which have $|S/DS| \geq 3$.

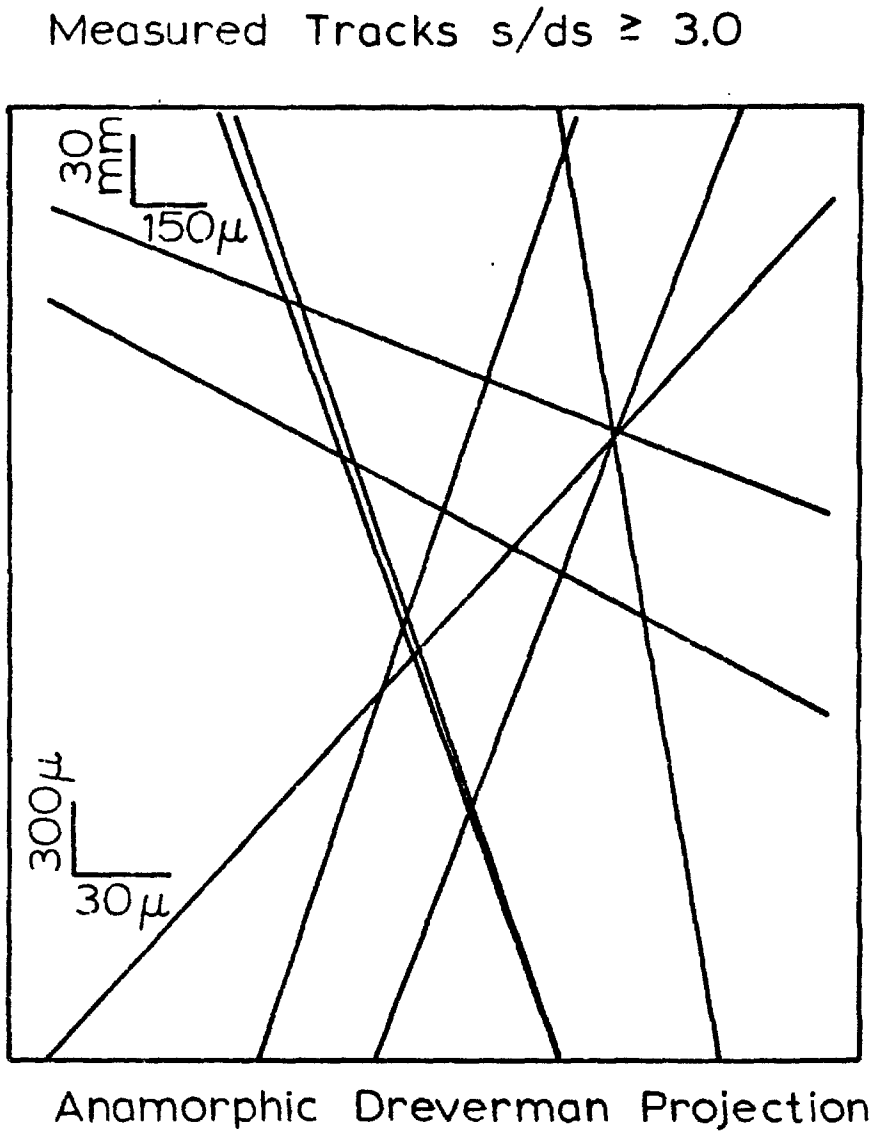

Figure 5-7: An anamorphic perspective plot of the measured tracks, in the selected $B\bar{B}$ event, which have $|S/DS| \geq 3.0$ relative to the primary vertex and which are not part of the four track vertex shown in figure 5-6

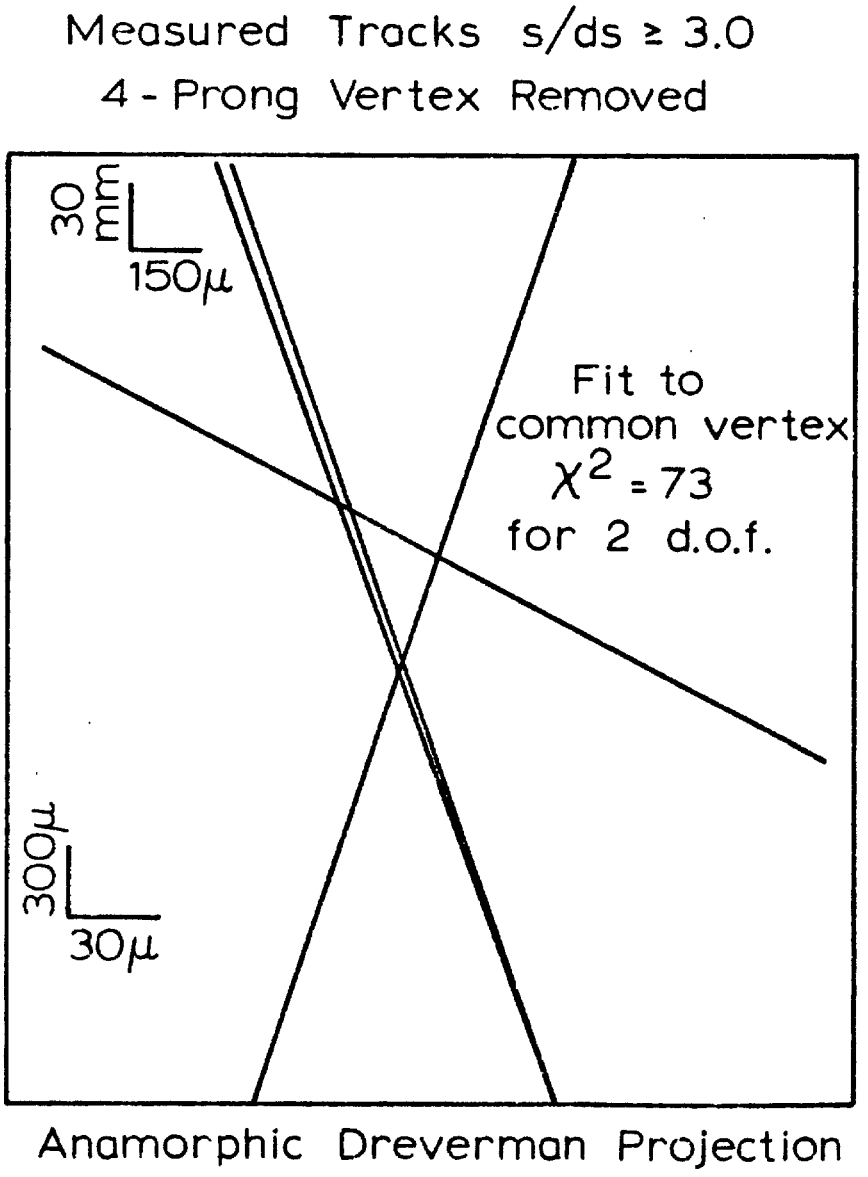

Appendix I

Hologram Analysis

Introduction

This experiment proposes to analyse a large number of holograms. Techniques to scan and measure have been developed in Europe in the NA25 collaboration. Building on this experience we can confidently predict the effort needed to build holographic scanning and measuring devices and the scanning effort involved. Several members of the NA25 collaboration have expressed interest in the present proposal and could join in at a later stage.

For the scanning and measuring of the holograms the NA25 collaboration uses two different approaches. One approach, mainly pioneered at CERN, uses television cameras to analyse the pictures. It is described in detail in [16]. The other method; pioneered in Brussels, uses direct projection of the image on a table as in an old fashioned scanning table. Both systems have similar performances as far as scanning speed and scanning and measuring quality is concerned. We tend to prefer the Brussels system which is simpler.

The second and third sections below describe the Brussels hologram scanning and measuring system, the fourth contains a cost estimate, and the fifth section discusses scanning and measuring speeds achieved.

Description of the Brussels Holographic Scanning System

The hologram scanning and measuring system was designed accoring to the following considerations:

1. The system was built for the NA25 CERN experiment which uses in-line holograhic recording, but it had to be made flexible and

should easily accomodate different holograhic recording schemes, e.g. side-band holography.

2. Direct optical projection gives an image which is by far superior to a TV image. All the scanning work should hence be done on the projected image as with a conventional scanning table. Nevertheless a TV image should be provided since it is often useful to superimpose computer generated information on the image, and this is most easily done on a TV image.

3. The optical projection system should have an intrinsic optical resolution of ~ 5 μm and the measurement precision of the system should be ~ 1 μm.

To achieve these goals we adopted the system shown schematically in figure I-0. It consists of an optical bench made out of standard Macro Bench components from Spindler and Hoyer [17] and a custom built precision X-Y-Z stage [18] which carries the hologram on one frame and a separate frame with a projection table and an operator's console. The optical bench can easily be reconfigured to allow for a different optical lay-out. The stage is equipped with Sneeberger [19] MK6-310 guidings and Steinmeyer [20] roller bearing with Heidenhain [21] linear encoders LS701 with 1 μm least count. The holograms are recorded on film. The holographic image is certainly more sensitive than a conventional image to distorsions of the film backing. Tests have shown however that with a strong film backing like the 170 μm thick mylar used here there are no particular film handling problems [22]. Nevertheless, we have developed a film transport system with very smooth movements. The film transport is on a separate stage which follows the X-Y-Z stage in one horizontal direction. An asynchronous motor on each reel keeps both ends of the film permanently under a constant tension. A sensor arm measures the amount of film on each reel and adjusts the torque of the corresponding motor such that the film is more or less in quilibrium even if one reel is full and the other is empty. This motor

can be controlled manually or by high level computer, but this last possibility is not yet implemented.

Exerience shows that in a holographic system one should reduce as much as possible the number of optical components. Each optical component will produce some reflections or scatter some light on dust particles. This light will interfere with the main illuminating light and produce interference fringes in the image. Antireflective coating on the lenses reduces this noise, but improper cleaning can easily damage such an antireflective coating and make it worse than an uncoated surface. Our system uses a beam expander which enlarges the beam to ~ 2 cm. A fixed projection lens (Cerco-f = 40 mm) [23] provides a magnification of 84 on the projection table. The laser is a Specta Physics water cooled argon-ion laser [24] which provides up to 1.8 W of power in the green 514 nm line. We use typically 200 mW of power for comfortable scanning.

The operator console consists of a projection table, a function keyboard, a computer terminal screen and keyboard, an X-Y trackball, a Z wheel and a manual film transport command knob.

From the point of view of the operator, the scanning of holographic images proceeds exactly the same way as the scanning of conventional images except that the operator has a Z wheel which allows him to focus on points at a different depth in the chamber. The total image presented to the operator measures 70 x 180 cm. Figure I-1 shows part of an image of a high energy interaction in a heavy liquid bubble chamber as it appears to the operator. This picture appears at a size of 42 x 30 cm^2 on the operators

rojection table. This corresponds to 4 x 3 mm^2 in space.

Electronics and Software

The electronics of the Brussels holograhic scanning table is derived from the CERN Bessy Matic control system [25]. It uses a MIK11-2C intelligent CAMAC crate controller [26] which offers all the power of the LSI-11 microcomputer from DEC and the flexibility of a CAMAC system. Interrupts are generated by CAMAC Lams and priority queues are handled by a clock interrupt system.

The motors of the stage and the film tranport system (ARTUS T-1342) [27] are driven via a CAMAC DAC module (SEN-9091) [28] and a power amplifier based on the RCA HC2000H circuit. The signals from the encoders are recorded with two CAMAC dual encoder modules (SEN-2019).

The control software in the MIK-11 consists of two modules representing 5K words of code written in assembly language. An EPROM resident module is assigned the basic communication tasks: link to host computer, downloading of program from the host and handling of the terminal. The module responsible for the control of the device hardware is maintained and cross-assembled in the host computer, a DEC-20, and down loaded in the RAM memory via a RS232 CAMAC serial line interface. In normal operation mode the MIK-11 appears essentially transparent to the user, as it mainly acts as an interface between a Fortran scanning/measuring steering program running on the host computer and the opertor's console terminal and functional keyboard. Indeed, except during initialization and termination f the scanning session, any character string typed at the terminal keyboard is simply passed to the steering program. Similarly, depressing a

key from the functional keyboard always transfers to the host the ASCII conversion of the selected key number, the X, Y and Z coordinates, and a device status word. ASCII strings received from the host, however, are interpreted by the microcomputer and either simply displayed on the terminal screen or used to activate device functions like initialising constants, moving the stage, enabling functional keys, moving the film transport (when implemented).

The control software also has the essential function of providing a feedback system for keeping the position of the X-Y-Z stage on a target value. This target may be modified either from the receipt of pulses generated by the movements of the X-Y trackball and Z wheel, or a request issued by the steering program running on the host. In both cases, the motors drive the stage to the new target value with a strength proportional to the distance from the target. To avoid oscillations the speed of the stage is estimated from the encoder pulse train and a signal proportional to the speed is algebraically subtracted from the DAC signal which drives the motors. This counteracts the movement to simulate ideal friction, the amplitude being adjusted such that the system is critically damped.

Cost Estimate for a Holograhic Scanning and Measuring System

The scanning device described in the two previous sections was designed and build in the Inter-University Institute for High Energies during 1981-1982. Part of the work was done in the Institutes workshop and part was given outside. The total cost in 1984 prices is estimated to be $100,000. The manpower involved is - 1 man year for a technician. This does not include the designing work or the programming which are freely available to the collaboration. The company which has suplied parts of

this system is offering a complete system on a commercial basis.

Experience with the Brussels Holographic System

The Brussels holographic system has been in operation for about 8 months and a total of 6000 holograms have been analyzed so far. The recording conditions for these holograms are described in refs. [29], [30]. The scanning speed achieved for NA25 pictures is probably a good approximation for what we can expect for this experiment since both experiments aim at finding charm and bottom decays in hadron interactions at high energies. In NA25 50% of the holograms do not contain an interaction which correponds to the trigger and is in the fiducial volume. Eliminating those holograms is very fast. If an interaction is found it is carefully checked for the presence of a secondary activity. One point is measured on each vertex, and on each secondary decay track. Two independent scans are made and the ifferences are checked on the scanning table for final decision. The table is used seven hours per day and 4 days per week. A total of 8000 holograms per year can be processed in this way on one table in one year.

From the NA25 experience one can safely conclude that, with the right equipment, holograms can be analyzed as easily as conventional streamer chamber pictures.

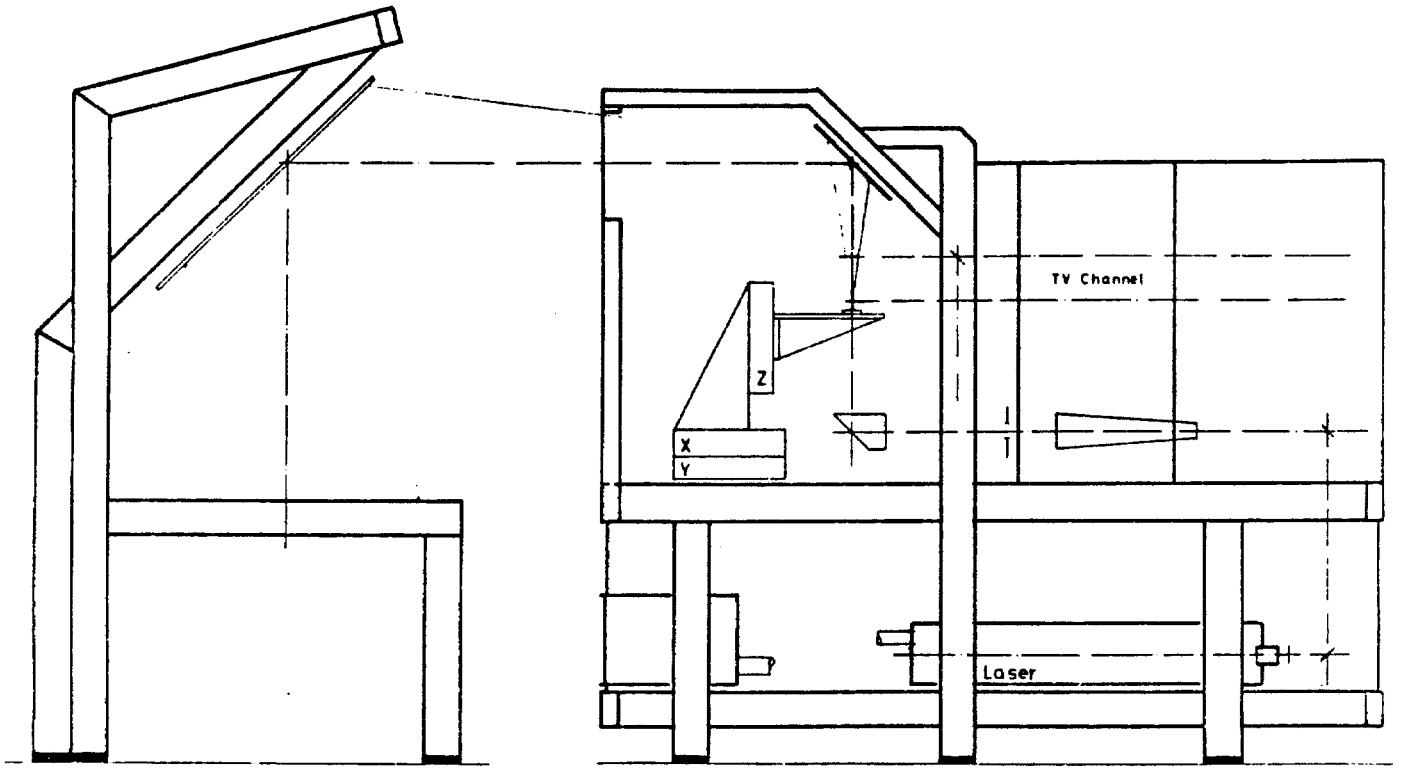

BRUSSELS HOLOGRAPHIC SCANNING AND MEASUREMENT TABLE

Figure I-1: Schematic representation of the Brussels holographic scanning and measuring system.

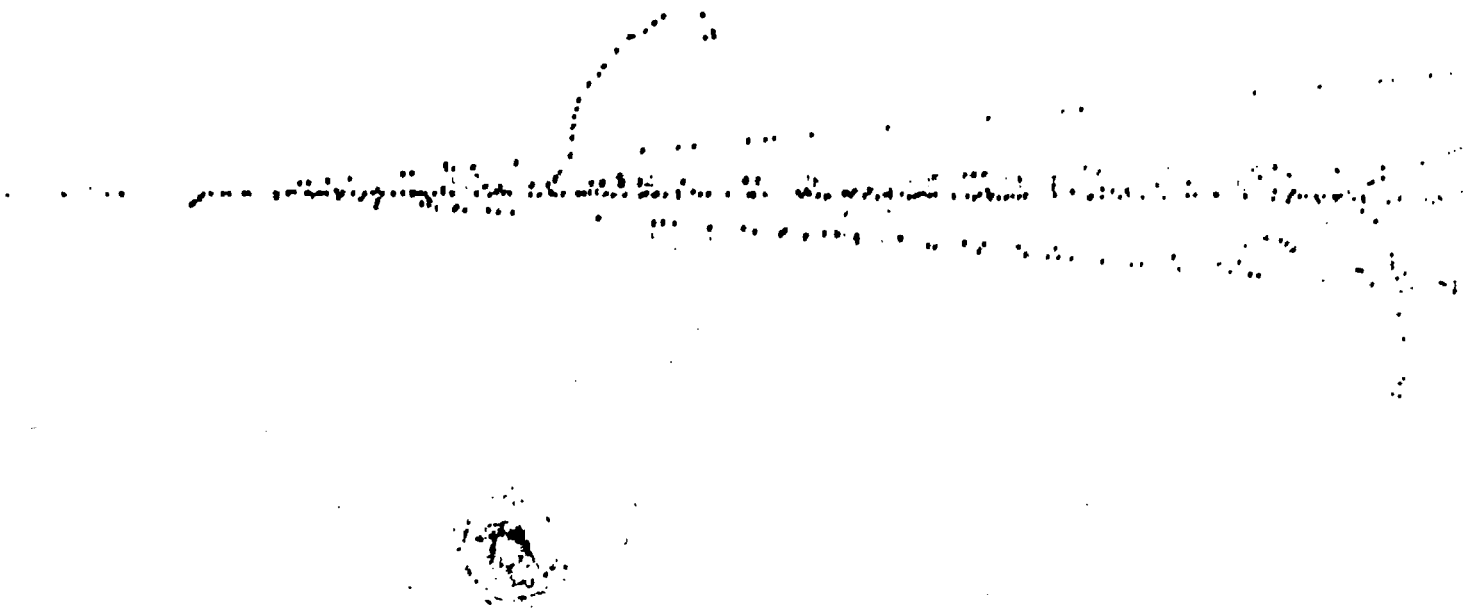

Figure I-2: Part of a picture of an event as it appears to the operator at the scanning table. This picture corresponds to 42x30 cm^2 on the table and to 3x 4 mm in space. The total image presented to the operator is 70 x 180 cm^2.

Appendix II

Trigger Processor

Overview

The design criteria for the trigger processor are:

1. Find tracks in the TRD and calculate P and P_{perp} for these tracks.
2. Reject tracks which fail the P cuts or P_{perp} cuts.
3. Compare the calculated P with an energy computed from relevant cells in the calorimeter and reject tracks which do not satisfy the $P = E \pm \delta$ criterion.
4. The results of all calculations and cuts should be available to form a trigger within a few microseconds after the interaction.

We present a scheme which accomplishes these goals using currently available technology. This is not intended to be a complete detailed design, but rather to show feasibility and to set the scale of the trigger processor.

We will deal with 3 stations of TRD PWC'S, each station having 2 mm spaced anode wires measuring in the bend direction of the magnet (X), plus cathode readout to measure in the non-bend direction (Y), and in a third (ambiguity resolving) direction (U). For illustration, we will take the third coordinate to be at 45° to the other two, and we will take the three stations to be equally spaced along the beam direction. (These choices do not affect the structure of the processor). We label the stations and coordinates as X^1, Y^1, U^1, for the upstream station, X^2, Y^2, U^2 for the middle station, X^3, Y^3, U^3 for the downstream station. In addition, we will consider an EM calorimeter with a cell structure such as described in the section on the apparatus. The architecture of the processor we describe can easily accomodate arbitrary directions of TRD PWC coordinates (as long as

one coordinate measures in the magnet bend plane), arbitrary TRD module spacing, and arbitrary EM calorimeter cell size and configuration.

Since the processing of the TRD data is the most complex part of the processor, we will start with this part.

To find a track in one coordinate projection (X for example), one looks for hits in the chambers which satisfy:

$$\left|\frac{X^1+X^3}{2}-X^2\right|<\varepsilon \qquad (2)$$

Similarly, to find a space point in a chamber station, one looks for hits satisfying:

$$|X+Y-\sqrt{2}U|<\varepsilon \qquad (3)$$

These equations have the same form, so one type of processor may be used for both.

Since a 2 mm spacing wire chamber 2 m long has 1000 wires, 12 bit accuracy for the arithmetic in the above equations will be adequate. A 12 bit add can be done in ~ 15 ns and an 8 bit comparison in ~ 5 ns. Calculations and Monte Carlo indicate the average event will have ~ 2 tracks (one decay electron and 0.7 electrons from an upstream conversion) plus ~ 1 hit from hadrons in the first chamber and ~ 2 hits from hadrons in the third chamber. We will consider a processor that can handle up to 10 hits in each coordinate. To test equations 1 or 2 for the worst case will require 10 x 10 x 10 = 10^3 computations. Even ignoring any propagation delays this would imply 10^3 x (10ns+5ns)=15μs for this part of the

computation if it is done completely serial. We would like to cut this by at least a factor of ~20, so we must do some computation in parallel. A natural break up of the problem is to do all combinations of two of the terms of equation 1 or 2 in parallel, and the third term in series. This requires a processor with 10 x 10 = 100 elements or cells which will have up to 10 cyccles.

Fig. II-1 shows the data flow for the TRD data and electron processor. Data from the chamber encoders is fed in parallel to a buffer for eventual computer readout (if the event is accepted) and through memory lookup units which apply scale factors and offsets to register banks which will then hold appropriately scaled quantities for the various calculations. There are three main processors which find X tracks, Y tracks, and space points (XYU match) in one chamber. In these processors a high degree of parallelism is used (see description below). A set of priority gates and chained lookups then fetches associated X and Y tracks and passes the relevant hit numbers to a section which calculates the kinematic quantities (P, P_{perp}, P-E) and applies cuts for each valid track. Data from the beam chambers and calorimeter are also made available to this section in the appropriate form.

Track Finder

We now look at the details of the track finding processor. Fig. II-2 shows the conceptual organization of such a processor -- specifically for the problem of finding tracks in the X coordinate. As mentioned above, the data for hits in the first and third chambers is fed simultaneously to the processor. This means each cell in the processor is computing eq. 1 for a different combination of X^1 and X^3 hits. The hits in X^2 are fed serially

into all cells at once, so that the number of cycles required is just the number of X^2 hits.

Eq. 2 may be rewritten as follows:

$$\left|\frac{X^1+X^3}{2}-X^2\right|<\varepsilon$$

$$|X^1+X^3-2X^2|<2\varepsilon$$

$$-2\varepsilon<X^1+X^3-2X^2<2\varepsilon$$

adding 2ε:

$$0<X^1+X^3-2X^2+2\varepsilon<4\varepsilon$$

Thus, one can feed X^1 hits and X^3 hits into the processor directly, $(-2X^2+2\varepsilon)$ can be "computed" by the memory lookup in the data stream between the chamber encoder and the "X^2" registers (which now store $(-2X^2+2\varepsilon)$ in the processor. Then, the result of the additions must only be checked to see that it is positive (high order bit(s) are used as a veto) and less than 4ε (magnitude comparison). (One may note here that if the TRD modules are not equally spaced along the beam line or if the TRD PWC stations do not have the "non-bend plane" coordinates at 90° and 45° as assumed above, this only changes the constants in eq. 2 or eq. 3. Since these constants are applied by memory look up units which are downloaded, this has no affect on the structure of the processor.)

A typical cell is shown in fig. II-2. with some IC numbers which indicate

components with adequate speed.

Further parallelism is achieved by having three of these 100 cell processors -- one for finding X tracks (as illustrated above), one for finding Y tracks (identical to the X track problem) and one for matching X-Y-U space points in a chamber (also identical to the X-track problem -- with different constants applied by the memory lookups in the input data steam).

As shown in Fig II-2, all hits from two coordinates are presented simultaneously to a 100 cell processor while the hits from the third coordinate (X^2, Y^2, or U^1) are cycled though -- each one being presented to all 100 cells. Any time a cell finds a good combination, a "valid" bit is set in that cell. After cycling through all the third coordinate hits, the information needed to associate X^1, X^3, Y^1, Y^3 hits on a 3-D track is contained in these "valid" bits. At this point, suitable token passing (priority encoding) and strobing is used to associate the valid track data. This process is a series of four chained lookups, where the quantities (data and addresses) involved are 10 bit numbers with only one bit asserted. This asserted bit position is just the number of the particular chamber hit to be used for this track.

At this point, the hit number gates of the three processors have a valid set of X^1,X^3,Y^1,Y^3 hits (hit addresses in the 10 bit form described above) for a good track. Of course, if any of the four coordinates does not have a valid hit on the track, the track is rejected.

Kinematics Calculations and Cuts

The hit numbers for a valid track found as described above are passed to the calculator section which computes P, P_{perp}, and P-E. This section has its own banks for storing the actual coordinates of the chamber hits. These banks have been loaded through their own sets of memory lookup units (and an adder for X^1-X^b, X^b=beam position), which apply appropriate constants. We calculate P and P_{perp} using an expansion which keeps only the linear terms in P_{perp}/P:

$$K = \frac{1}{P} = \frac{H(X^1-X^b)-(E+D+G)(X^3-X^1)}{(H*D/\alpha)(D/2+E)} \tag{4}$$

$$P_x = \frac{(X^3-X^1)+D*K*(D/2+G)/\alpha}{H*K} \tag{5}$$

$$P_y = \frac{Y^3-Y^1}{H*K} \tag{6}$$

$$P_{perp}^2 = P_x^2+P_y^2 \tag{7}$$

The geometric constants H, E, D, G are defined in Fig. II-3. The constant α is related to the magnetic field ($\alpha=(.0003B)^{-1}$). Eq. 4 can be written:

$$K = a(X^1-X^b) - b(X^3-X^1).$$

The banks in the calculator section will have the quantities $a(X^1-X^B)$ and bX^3, bX^1 stored in them so that eq. 4 may be calculated with 2 addition cycles.

Eq. 5 can be written:

$$P_x = \frac{(X^3-X^1)}{H*K} + C$$

The coordinate banks will also have X^3 and X^1 stored so that while the additions for eq. 4 are being done, X^3-X^1 can be computed. Since C is constant, having (X^3-X^1) and (K) determines P_x. The division required $((X^3-X^1)/K)$ can be done by memory lookup. This memory lookup will give P_x as a function of K and X^3-X^1 and will require only one lookup cycle after the two additions to compute eq. 3. A similar lookup can be used to generate P_y as a function of (Y^3-Y^1) and K. Finally, a lookup can be used to generate a yes/no (P_{perp} cut) as a function of P_x and P_y. To get this yes/no bit then requires two lookup cycles plus two addition cycles for each valid track (X^1,X^3,Y^1,Y^3). (One may note here that if the TRD PWC's do not have a coordinate measruing in the "non-bend plane", the processor will be identical up to the point of calculating P_y. To get the Y coordinate, one extra addition will then be required. This can be done in parallel with the (X^3-X^1) calculation required for P_x so it will not require any extra time.)

After calculating equation 4, the P cut can also be applied by comparators or memory lookup. This will require only one cycle after equation 4.

The remaining cut on the electron is P-E (where P is the momentum calculated above, and E is the energy from the EM calorimeter). To perform this cut rapidly, we would store the calorimeter data in a form which can be accessed rapidly once the track parameters for an electron candidate are

known. At the same time, we do not wish to place excessive constraints on the calorimeter element size or configuration.

One can envision a rectangular (X-Y) grid superimposed on the calorimeter face. For each grid cell one determines which calorimeter elements could contribute to the measurement of the energy of an electron entering the calorimeter in that cell. The signals from those elements can be added (analog) and the sum digitized with a flash ADC and stored in a register whose address is just the X-Y location of the grid cell. Any track may be projected to the calorimeter face (two additions -- or if the third TRD chamber is close to the calorimeter, just use its coordinates). This projected position -- X^{cal}, Y^{cal} can be used to address the register containing the corresponding energy sum (possibly with one memory lookup to scale X^{cal} and Y^{cal} to the calorimeter grid system). If one uses a 5 cm cell size, for a 2 m x 1 m calorimeter one will have 800 cells. One subtraction and one comparison is required to make a cut on P=E.

Trigger Delay Time

We now estimate the time required to form a trigger with the above scheme. We let t_o be the time of passage of the particles through the detectors. We ignore here the ~50 ns traversal time for the length of the apparatus. For the TRD, ~400ns drift time will be required for there to be adequate discrimination between minimum ionizing tracks and transition X-rays. There will also need to be about 200ns cable delay to form a pretrigger. The hits in the TRD chambers will be encoded in: 30ns x (no. hits = 4 on ave.) = 120ns. We can assume that the data will be in the track finders in: 400+200+120=720ns after t_o. We will take 800ns for this number.

The track and space point finders require one cycle to compute the first addition plus one cycle (addition plus compare) per X^2 (Y^2,U^1) hit to find all projected tracks and all space points in the first chamber. Since additions can be done in 15ns, and comparisions in 5ns, we will take 30ns per cycle. (This allows time for data setup). On average there will be 3.5 X^2 and Y^2 hits and 3 U^1 hits. We will allow five cycles or 150ns.

The longest calculation, once the tracks have been found, is P_{perp} which requires the serial calculation of P,(P_x,P_y) and P_{perp}. As shown in the text above this requires two additions plus two lookups. We allow 30ns for each of these four cycles (additions take 15ns, lookups take 25ns, plus some setup or propagation delay). Thus, 120ns per valid track is required for the P_{perp} calculation. In addition, some time is required to associate the X and Y tracks. This should take about 50ns - and is added only once, since the second track, if present, may be associated while P_{perp} is being calculated for the first track. The typical event of interest has two valid tracks (one decay electron plus one conversion electron), hence the track association plus kinmatics calculation will require (2 x 120) + 50 = 290ns.

The total time from when the particles pass through the apparatus to having a trigger decision is given in table II-1.

Of this time, 480ns scales with the multiplicity of hits or tracks in the event. Thus, allowing the number of hits in a plane to be 8 (instead of 4) and the number of valid tracks to be 4 (instead of 2) would increase the trigger time to 1240+480= 1720ns.

Table II-1: Time required to make trigger decision.

400ns	(TRD drift)	
200ns	(cable delay)	
120ns	(encode hits)	(30ns x # hits)
80ns	("contingency")	
150ns	(track finding)	(30ns + 30ns x # hits)
50ns	(track association)	
240ns	(P_{perp} calc.+cut)	(120ns x # tracks)
1240ns	Total "typical" event.	

Scale of the Processor

We now estimate the size of the processor based on the scheme outlined above. As shown in fig. II-2, the basic cell in the track finder requires eight chips for the adders, plus a comparator. We assume the gating required will add another 1 to 2 chips per cell. This should allow 10 cells per board (about 70W power per board). Hence, 10 boards (for 100 cells) plus ~2 more boards for control and diagnostics will complete one track finder. This is about one bin (< 1kW power). Three such processors will be required (three bins). (Note: Using a custom IC for one cell of the processor would allow putting an entire 100 cell processor on a board.) The memory lookup units are small and would probably be distributed throughout the processor (using the INMOS IMS1423 4k x 4 CMOS RAM would mean only 3 chips plus gating per look up unit). The flash ADC system for the calorimeter should require 2-5 bins. Thus, the entire processor will require 5-8 bins. Much of the system is highly repetative, so that the scale should be comparable to a PWC readout system.

Figure II-1: Block diagram of trigger processor showing data flow.

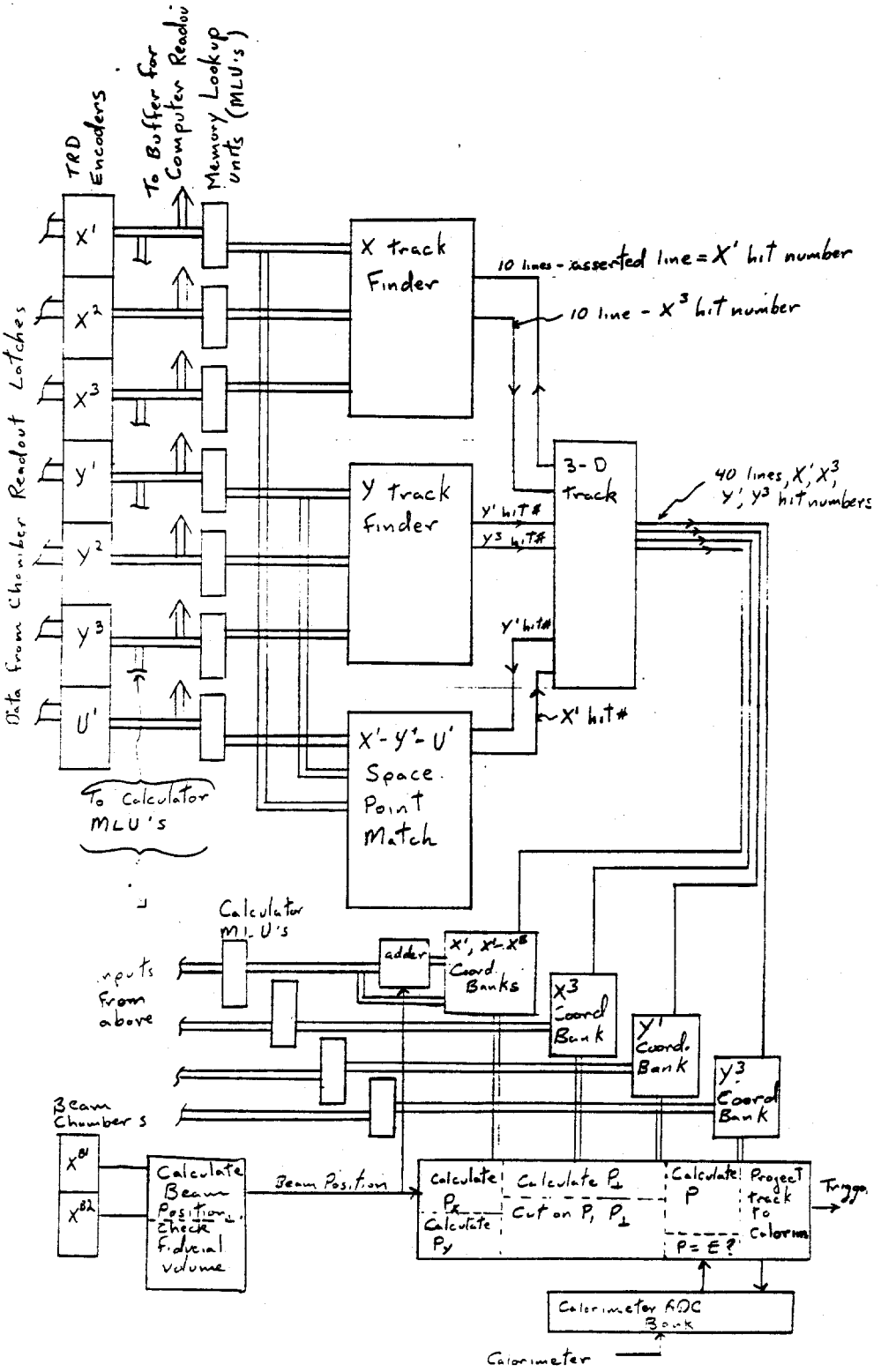

Figure II-2: Block diagram of 100 cell processor and detail of one cell.

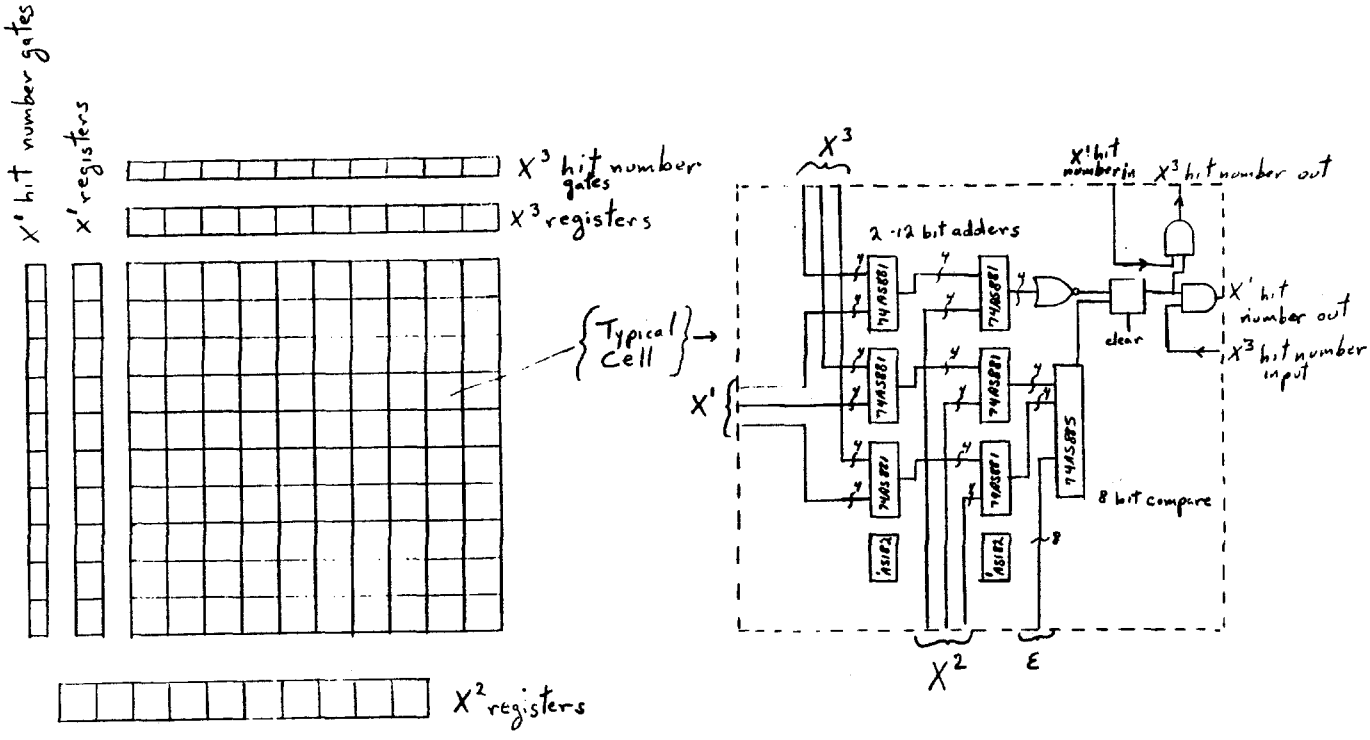

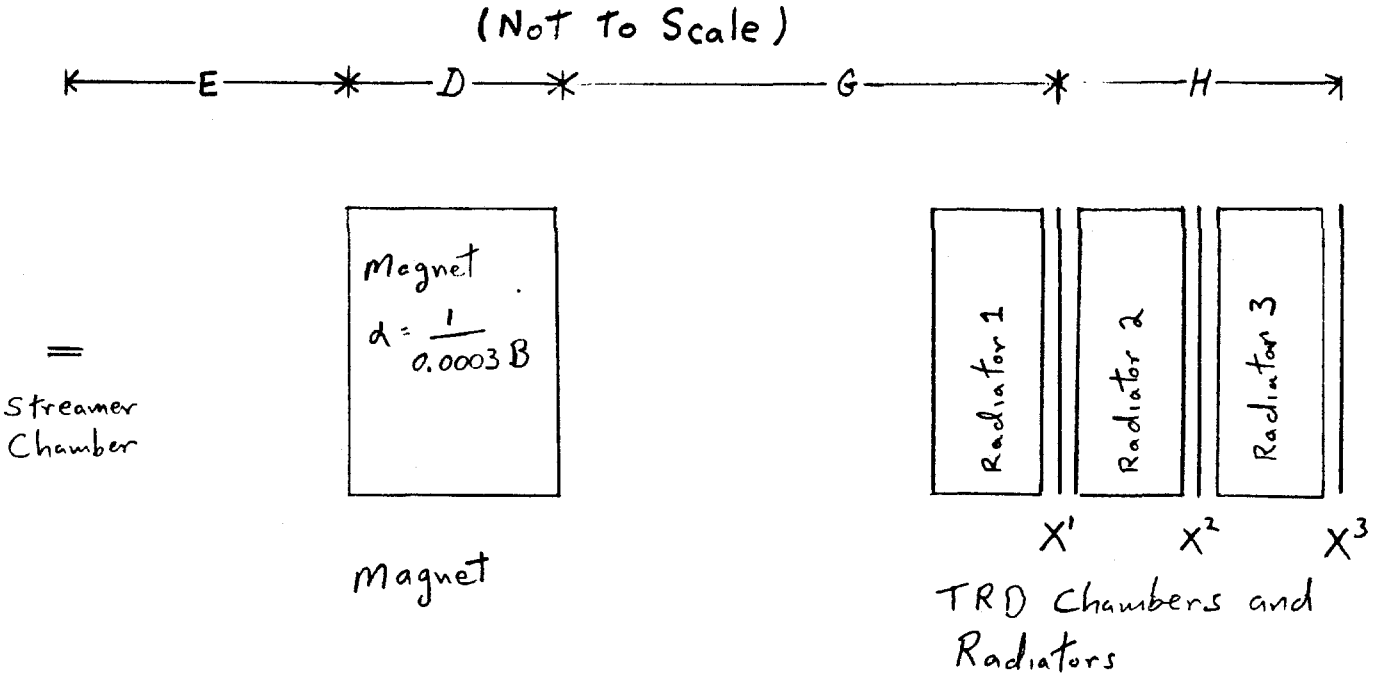

Figure II-3: Definition of geometric constants used in momentum calculation.

Appendix III

Streamer Chamber Research and Development

In 1982 the Yale group began a program to significantly improve the resolution of the high pressure high resolution streamer chamber (HIRSC) developed by this group.

The motivation and goals for this research program are outlined in the body of this proposal.

The great utility of a triggerable vertex detector with adequate resolution to resolve tracks of charm and beauty decays has been the driving motivation for the development of the HIRSC. The streamer chamber offers triggerability with memory time in the few microsecond range -- readily controllable by the addition of small amounts of electronegative gas such as SF_6. Prior to our work, however, streamer chambers operated at one atmosphere, with streamers about 1 mm in diameter and about 1 cm in length. Such chambers are not useful for studying charmed particles -- which even at Fermilab energies travel only a few mm before decaying. Detailed studies carried out by our group and others have shown that track widths must be less than 200μm to be useful for charmed vertex detection and track widths down to ~20μm are needed to realize the full potential of the method.

The past work of our group has developed the necessary technology for a high resolution streamer chamber (HIRSC) which operates at 40 atmospheres with tracks in the 120μm to 150μm (spatial) width range. This chamber has een used in Fermilab experiment E-630.

The goals of the development program for a second generation chamber are listed below.

1. Operation at pressures of 50-100 atmospheres. The increase of operating pressure, relative to the E-630 chamber pressure of 40 atmospheres, is primarily to increase the interaction rate. Since the chamber gas is the target, increasing the chamber pressure increases the interaction probability per incident particle. The increased pressure also results in an increase of streamer density (no. of streamers per centimeter of track).

2. A fiducial volume of ~10x5x1.5 cm^3. The increase of size (relative to the E-630 volume of 4x4x.5 cm^3) has two important functions. First, the interaction probability is increased, and second, the longer chamber dimension allows the forward jet of particles to separate and thus to be measured and correctly associated with the tracks found in the downstream detector.

3. Track width in the 20μm range.

To achieve these goals we have been pursuing a research effort at Yale that has several aspects. These include: holographic recording of streamer chamber tracks; suppression of the thermal diffusion of ionization electrons on tracks (the diffusion of electrons away from the track site in the time between the passage of the ionizing particle and the arrival of the high voltage pulse is the major source of track width in high pressure streamer chambers); construction of a new high voltage pulser; design of an experimental apparatus incorporating the high resolution streamer chamber, a highly selective trigger for interactions in the chamber in which charm or beauty particles are produced, and a sophisticated downstream spectrometer to analyze the events. We will summarize below the the results achieved to date and the expected near-term progress for the streamer chamber and associated systems.

Holography

We have been using the high pressure streamer chamber developed for E-630 to study holographic recording techniques for tracks in streamer chambers.

As of about one year ago, we were considering two possible approaches to holographic recording of streamer chamber tracks: using light scattered from the thermal inhomogeneity caused by the streamer, and using light resonantly scattered from neon metastable states formed in the streamer. The first method (thermal) was pioneered by Russian physicists and has been pursued by a group at CERN (Ekhardt et al) with which we have maintained a close collaborative contact. We began studies on the second method (resonant scattering)at Yale in January 1983. This method looked quite promising because of the potential to obtain a large scattering signal (i.e. high contrast). After several months of study however, it became clear that certain difficulties inherent in this method made it less practical to implement than the thermal method. In particular the rapid dimerization at high pressure of the excited neon atom to form molecules -- which do not have large oscillator strengths for any transition in the visible light range -- put very severe limitations on the gas mixtures one could use. During the time we were studying the resonant scattering method, work was proceeding at CERN on the thermal method. By May 1983, the group at Cern had recorded tracks with streamers ~ 30 μm diameter at 13 atmospheres (10% methane in helium). Starting in May 1983 we switched our efforts to using the thermal method. During the summer of 1983 we succeeded in recording tracks under a variety of conditions and gas mixes using this method. Table III-1 below summarizes the gas mixtures with which holgraphic recording was achieved.

In the fall of 1983 we purchased a 4 watt argon ion laser and associated optics and bench to set up a reconstruction laboratory for the holograms. his has allowed us to study in detail the properties of holographically

Table III-1: Gas Mixtures for Holographic Track Recording

Pressure	Mix
15 atm	10% CH_4, 90% He
15 atm	10% CH_4 81% Ne, 9% He
24 atm	6.2% CH_4, 84.4% Ne, 9.4% He
34.3 atm	4.2% CH_4, 86.2% Ne, 9.6% He
5 atm	10% CH_4, 90% Ar
11 atm	7-10% CO_2 in 90% Ne+10% He
30 - 35 atm	1% CO_2 in 90% Ne + 10%He
20 - 35 atm	90% Ne, 10% He

recorded tracks.

In summary, the results of the development of holographic track recording to date are:

- Visible tracks (on reconstruction) up to 35 atm in the existing streamer chamber.
- 5-10 streamers per millimeter visible on reconstructed tracks.
- Streamers as small as 8 μm visible on reconstructed tracks.
- Operation with a variety of gases (Helium, Neon, Argon).

Figure III-1 shows a photograph taken from a reconstructed hologram of a Ru^{106} β track in the E-630 chamber. This track was

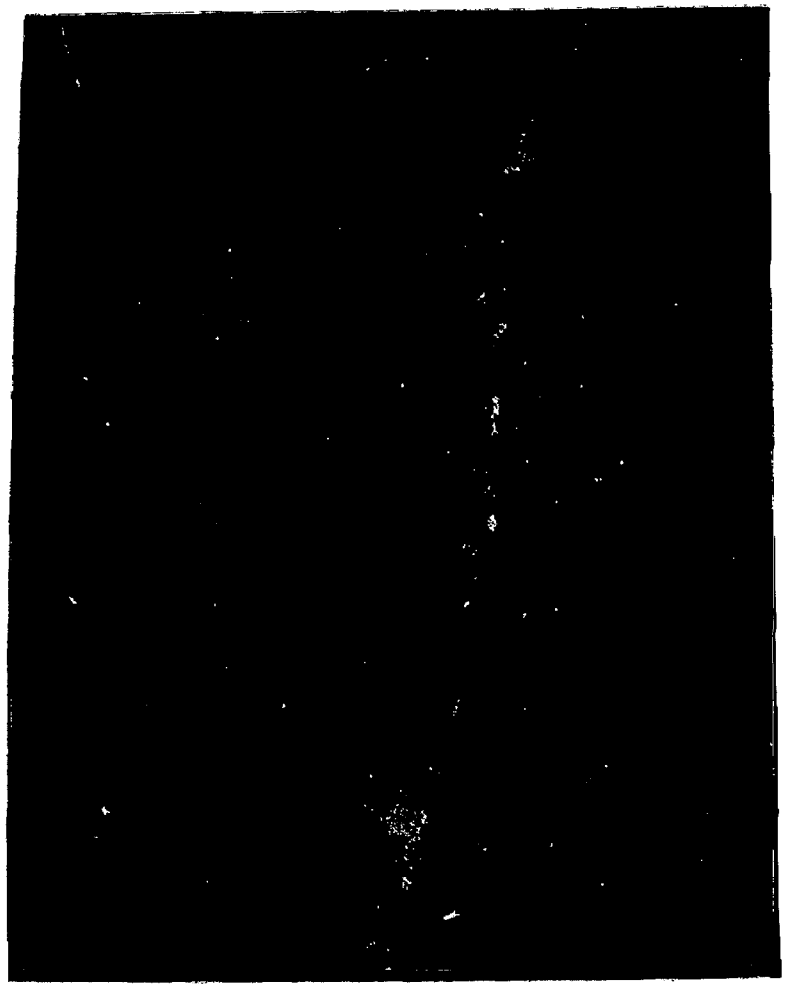

Figure III-1: Photographic reproduction of reconstructed hologram taken in E-630 chamber. Magnification = 9x.

obtained at a pressure of 31 atm (90%Ne,10%He, plus small amounts of CO_2 and CH_4). One can note that in the ~1μs required to form the trigger and apply the high voltage pulse to the chamber the ionization electrons have diffused to give a track full width of ~500μm in space. Since many of the streamers are very small and the diffusion occurs both in depth and width, many streamers are not in focus and hence are not recorded on the photo-reproduction. These streamers are still recorded on the hologram however and one can find them by scanning in depth (focus). Fig.III-2 shows a montage made by scanning the track

in Fig. III-1 in depth and recording by hand (tracing) all streamers found. There are 10.6 streamers per millimeter on this track. (One sholud note that tracks recorded using the diffusion suppression technique described below will be sufficiently narrow that the streamers will all be in focus at once.)

The major areas for further developmnet in holography are:

- Improvements in contrast -- particularly for small streamers
- Increase in the streamer density on tracks (20 per mm is a goal).

Our plans in these areas are summarized below:

1. Longer higher voltage pulse: The work at CERN indicates that this should make the streamers more visible. A pseudo-conical Blumlein which should give a 3 ns pulse(current chamber has ~1 ns) has been designed and is being fabricated.

2. Higher streamer chamber pressure: The new chamber will operate at ~2 times the pressure of our existing chamber. This means there will be 2 times the ionization density along the tracks. Also, the higher pressure means a larger index change in the region of the streamers which should give higher contrast.

3. Contrast enhancement: A scheme has been developed which should allow significant contrast enhancement in an in-line (single beam) holographic setup. This scheme involves using a set of transfer lenses between the streamer chamber and the film which

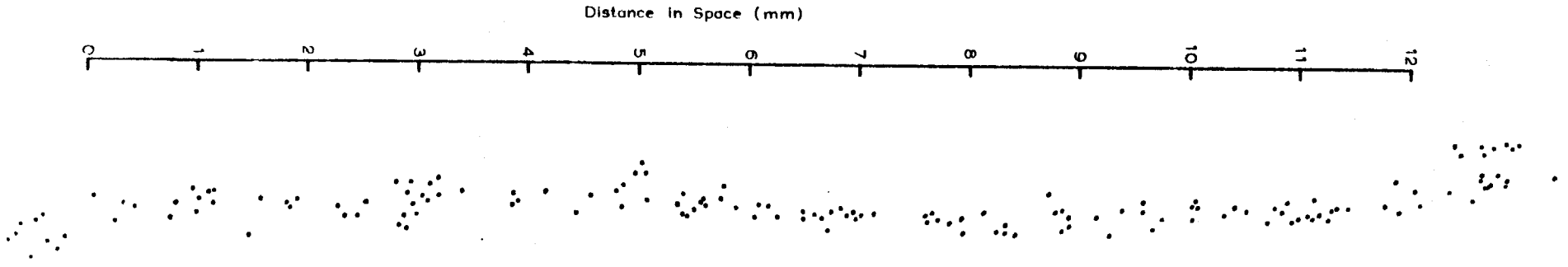

Figure III-2: Hand-drawn montage from scanning track in depth.

brings the main laser beam (reference beam) to a focus between them.(Fig. III-3) A small (<1 mm diameter) half wave plate at this focus is used to rotate the polarization of the reference beam. The light scattered by the streamers passes outside the half wave plate and is unaffected. A polaroid before the film aligned with the unrotated reference beam absorbs some of the (rotated) reference beam (the component rotated orthogonal to the polaroid axis) while transmitting the scattered light. This scheme allows arbitrary attenuation of the reference beam with respect to the scattered light while maintaining the advantages of inline holography (ease of setup -- by auto collimation, plus maximum signal by looking in the forward direction). We have contracted a commercial optics shop to produce the small half wave plate and will be testing this scheme this fall.

Diffusion Suppression

In November 1983 we focussed our efforts on finding a suitable technique for suppressing diffusion of the ionization electrons in the streamer chamber.

Our scheme is to try to attach the electrons to an electronegative molecule (such as oxygen) in a short time (a few tens of nanoseconds) before they can diffuse very far. The negative ions thus formed are relatively heavy and do not diffuse an appreciable distance in the time required to develop a trigger and apply the high voltage pulse to the chamber. Just before (~10 ns) applying the high voltage pulse to the streamer chamber the electrons can be liberated by photoionizing the negative ions with light from a laser. By adjusting the concentration of the electronegative gas one can adjust the electron capture time and hence adjust the time during which the electrons are "free" to diffuse.

To study this process, we are using a high pressure parallel plate ion chamber (Fig. III-4). An Americium source emits 4.3 MeV alpha particles which leave about 60,000 ionization electrons in the gas (90% Ne, 10% He,

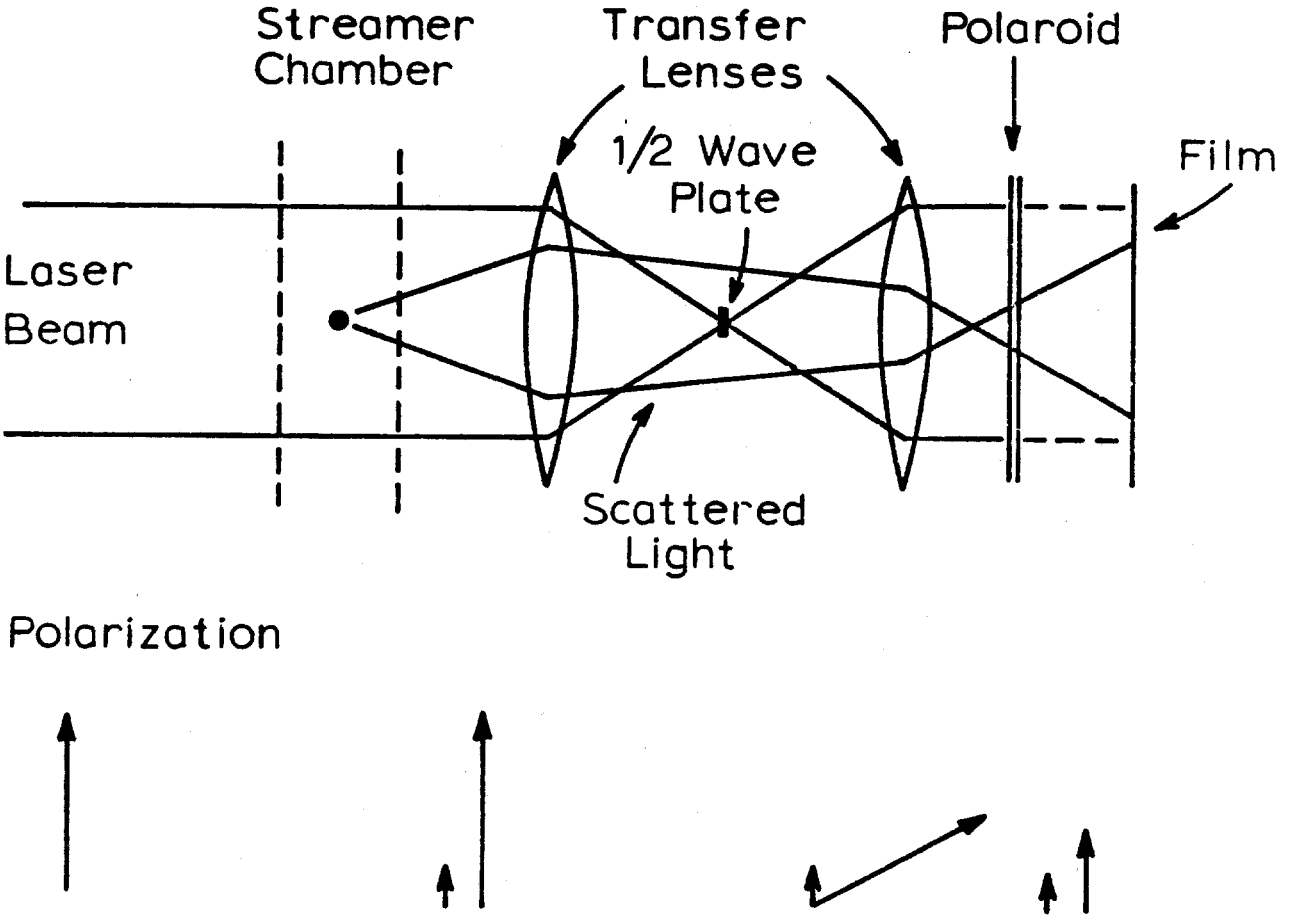

Figure III-3: Set up for contrast enhancement in in-line holography

plus small amounts of O_2). The drift of these electrons under the influence of the electric field induces a current flow between the electrodes which can be detected by using a charge sensitive amplifier. Adding oxygen to the neon-helium causes the ionization electrons to be captured as negative ions which drift much more slowly than the electrons. Hence the short time (few microsecond)pulse associated with the ionization is reduced. If one now shines a laser beam through the region where the negative ions have been formed, any photoionization can be detected by seeing a second pulse, after firing the laser, caused by the drift of the liberated photo-electrons.

The direction and goals for these ion chamber studies were:

- to have a chamber capable of operating at pressures near our design goal for the streamer chamber (50-100 atm);
- to have a vessel which could operate under very clean conditions (no plastics, capable of bake-out and glow discharge);
- to observe photoionization of the negative ions by visible light;
- to measure photoionization efficiency using several different wavelengths and power densities so as to determine the type of laser required for the diffusion suppressed streamer chamber.
- to observe the time evolution of the negative ions over a time period of ~ 10 μs so as to find a means of setting the memory time for the streamer chamber.

In the fall of 1983 we installed a 90 atm pressure vessel with a parallel plate ion chamber in our laboratory and began studies on the photoionization of negative oxygen ions with visible light. After several months of studies with green (λ=514 nm) and violet (λ=408 nm) light, including many refinements in the signal processing, it was clear that there was no photoionization signal.

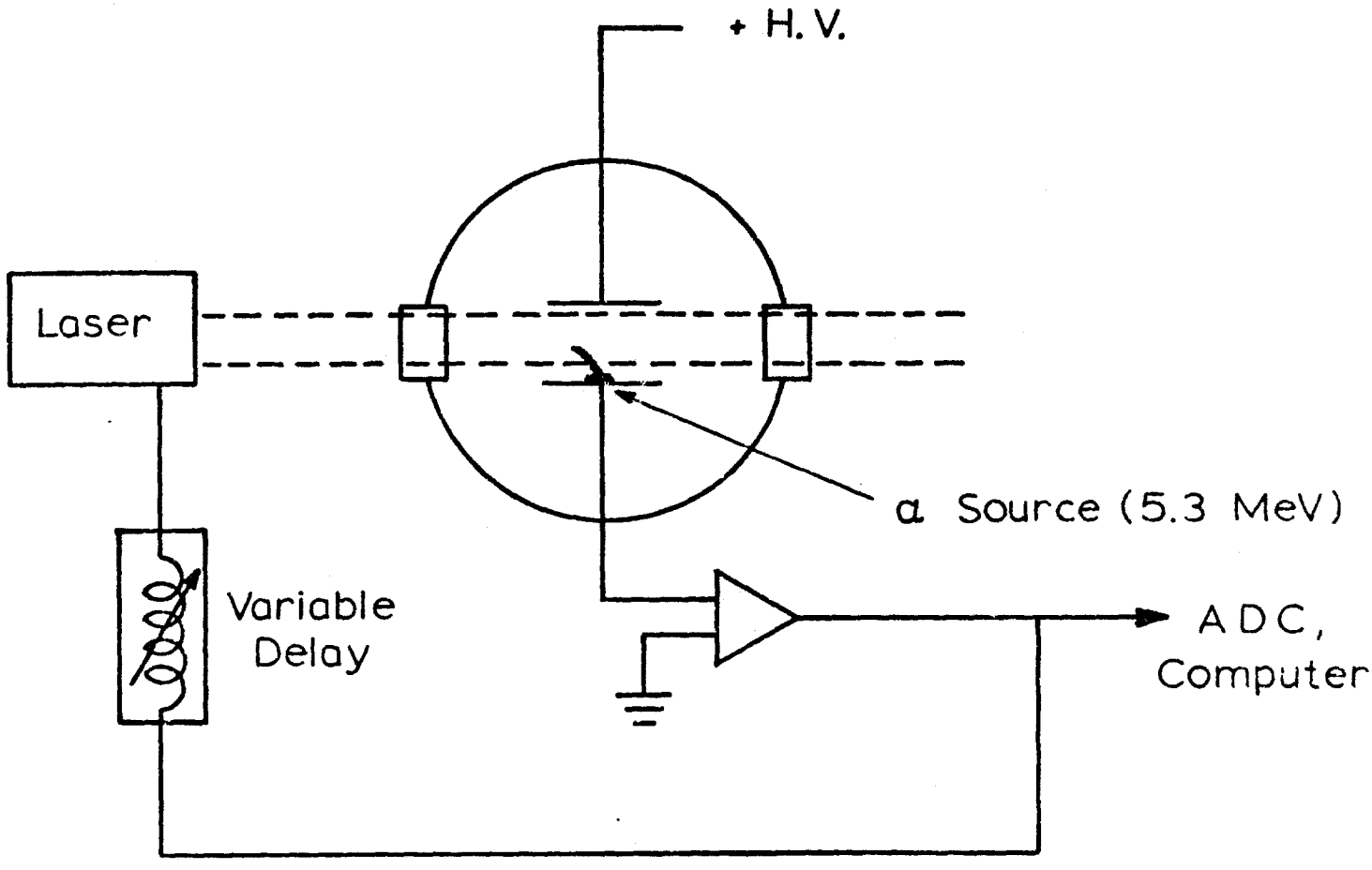

Figure III-4: High Pressure Ion Chamber for Negative Ion Studies

The cross sections for photodestruction of various negative ions are shown in Table III-2. It is not known what fraction of the photodestruction cross-section (for O_4^-, CO_4^-) is photoionization. Clearly at 406 nm (and also at longer wavelengths) O_2^- and O_4^- have significant cross sections while CO_4^- has a very small cross section. Also, there is a very high reaction rate for the process $O_4^- + CO_2 \rightarrow CO_4^- + O_2$. A few tens of microns Hg partial pressure of CO_2 would convert the O_4^- to CO_4^- in ~ 1 μs. This would quench the signal in our ion chamber. Professor William Chupka from the Yale chemistry department, who has given us invaluable consulting aid, informs us that this is a very reasonable level of contamination just from outgassing of metal walls. This is also a level of CO_2 that could come with the spark chamber gas (90%Ne, 10%He) we are using.

Table III-2: Photodestruction Cross Sections for Some Negative Ions (in MBarns)

	WAVELENGHT - nm	
ION	406.7	351.1
O_2^-	3.7	3.4
O_4^-	2.9	8.4
CO_4^-	?<0.06	0.45
$O_2^- \cdot H_2O$	1.2	2.6

In April of this year we modified the gas system of the ion chamber to allow bake out of the vessel to ~100°C, pumpout with a cryopump, and use of a gettering purifier on the inlet gas.

After implementing these changes we first observed a photoionization signal with visible light (408 nm, violet) in May of this year. Figure III-5 shows the size of the signal as the laser beam is scanned horizontally across the chamber. When the beam is above the source (in the region where ionization is produced) one expects a signal; however, there should be no signal when the beam is to the side of the source. This is what is observed. Figure III-6 shows the dependence of the photoionization signal on laser power. The linear dependence is characteristic of a single photon process. Figure III-7 shows the dependence of the photoionization signal on the laser delay after detecting the initial α-particle signal. The exponential fall off of the signal with time indicates that there is a chemical reaction going on which removes the negative oxygen ions from the gas. The gas in the chamber at the time of these runs had been in the chamber for four days. Figure III-8 shows the same lifetime curve after filling the chamber with fresh (purified) gas. The longer lifetime observed for the negative oxygen ions indicates that the contaminant which was reacting with the oxygen ions can be flushed out by changing the gas. For all these studies, the gas was 17 atm (90%Ne+10%He) plus 0.05 atm O_2.

A further test was performed by adding 100 microns Hg partial pressure of CO_2 to the gas. No photoionization signal was observed after adding the CO_2.

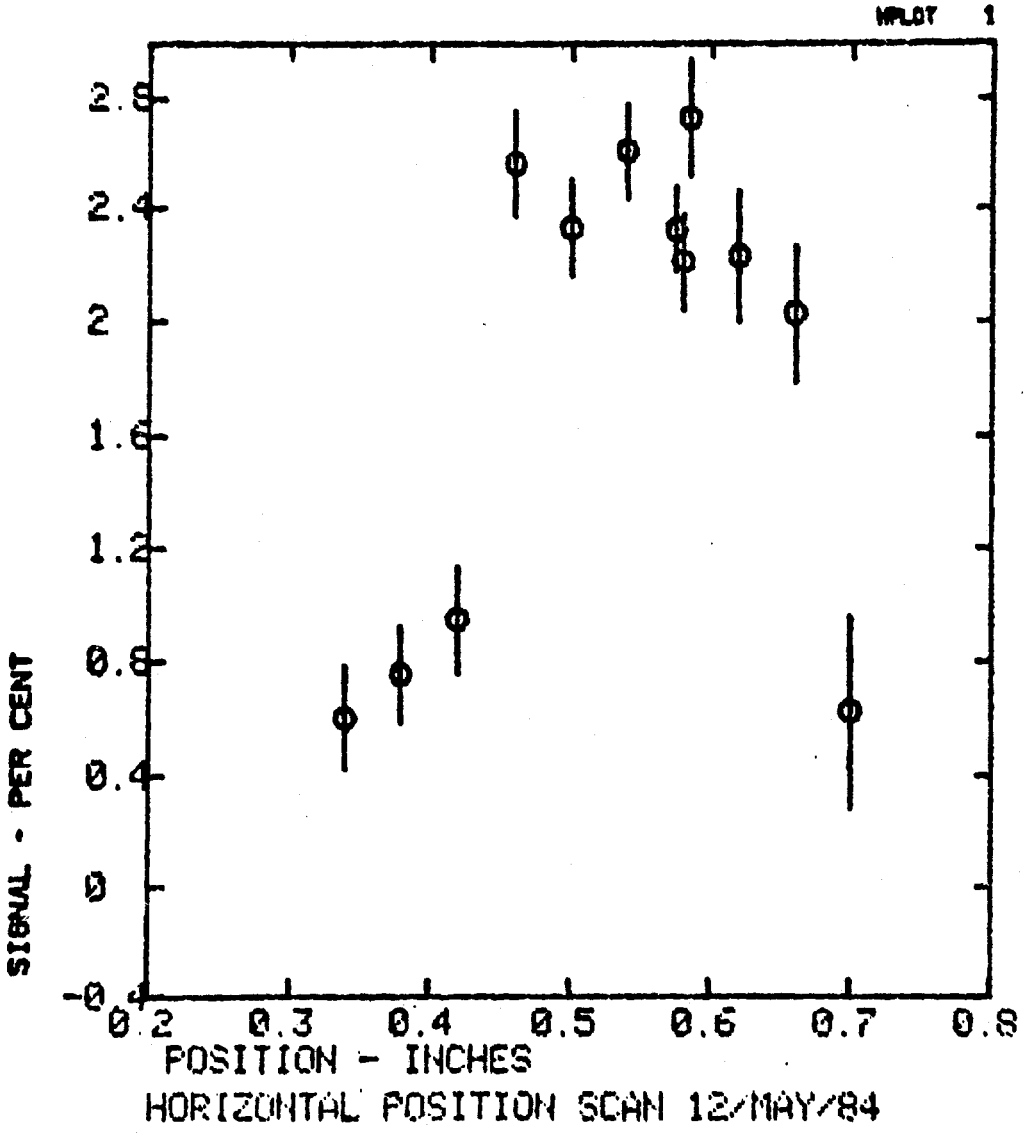

Figure III-5: Horizontal Scan of Laser Beam Across Ion Chamber

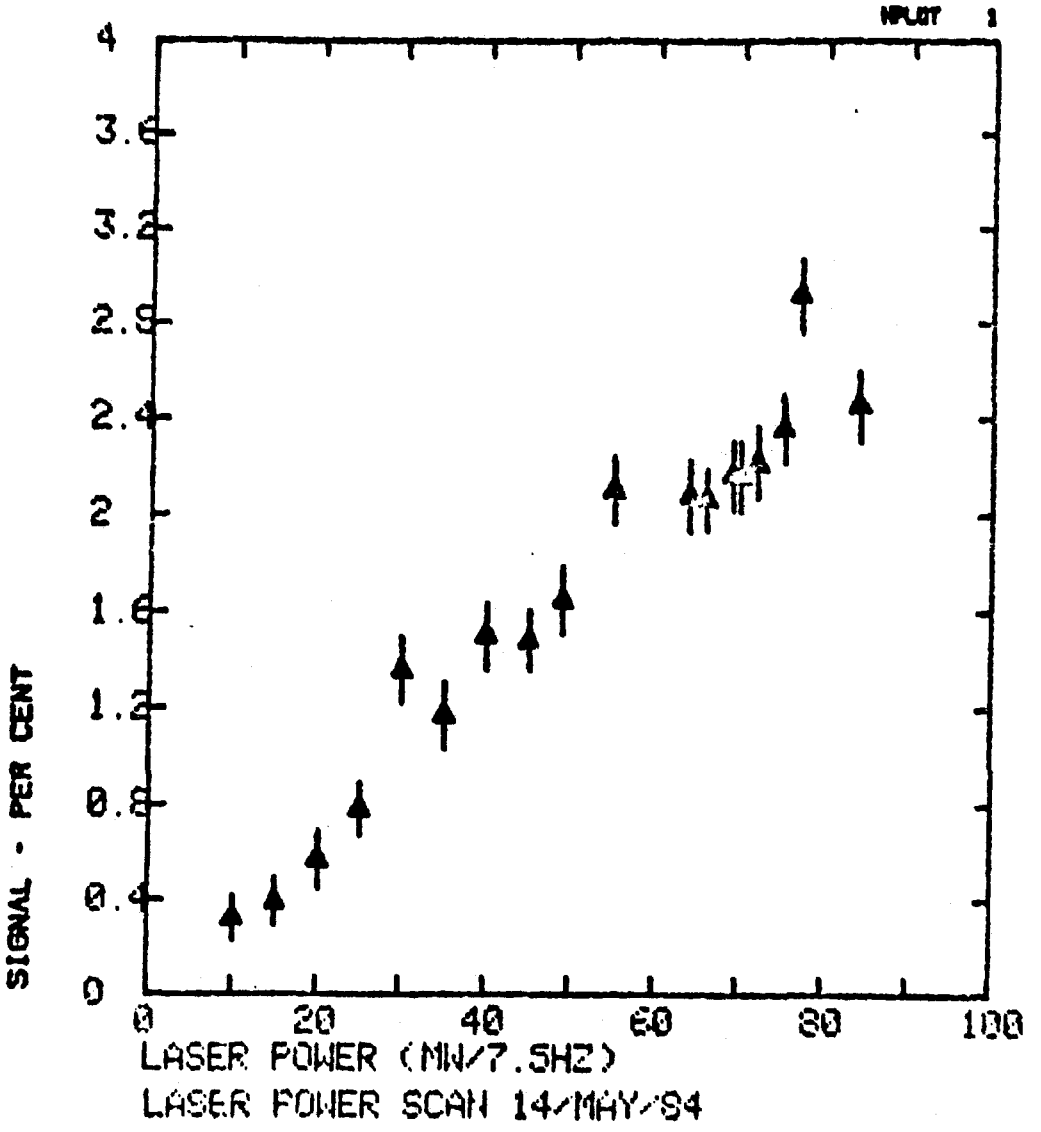

Figure III-6: Dependence of Photoionization Signal on Laser Power

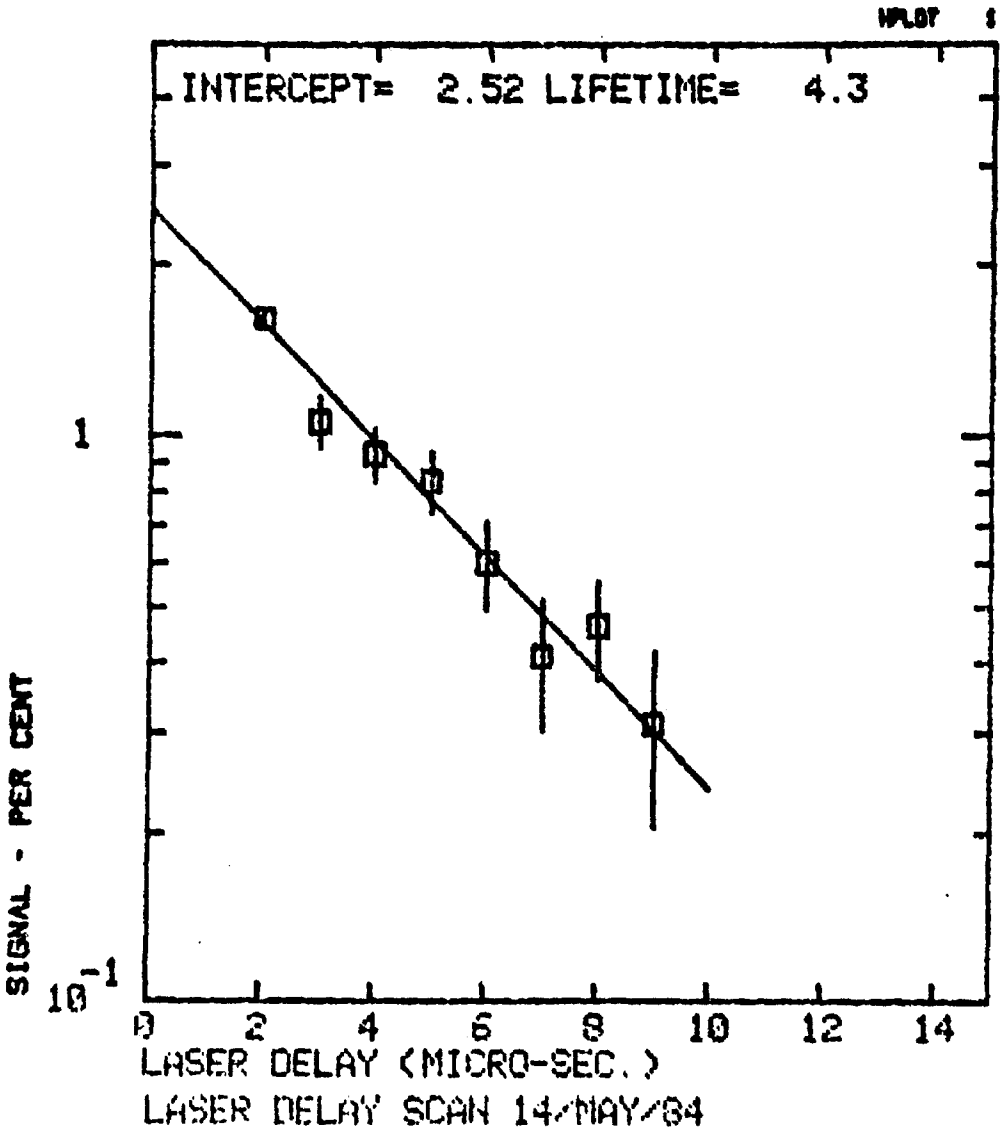

Figure III-7: Dependence of Photoionization Signal on Laser Delay

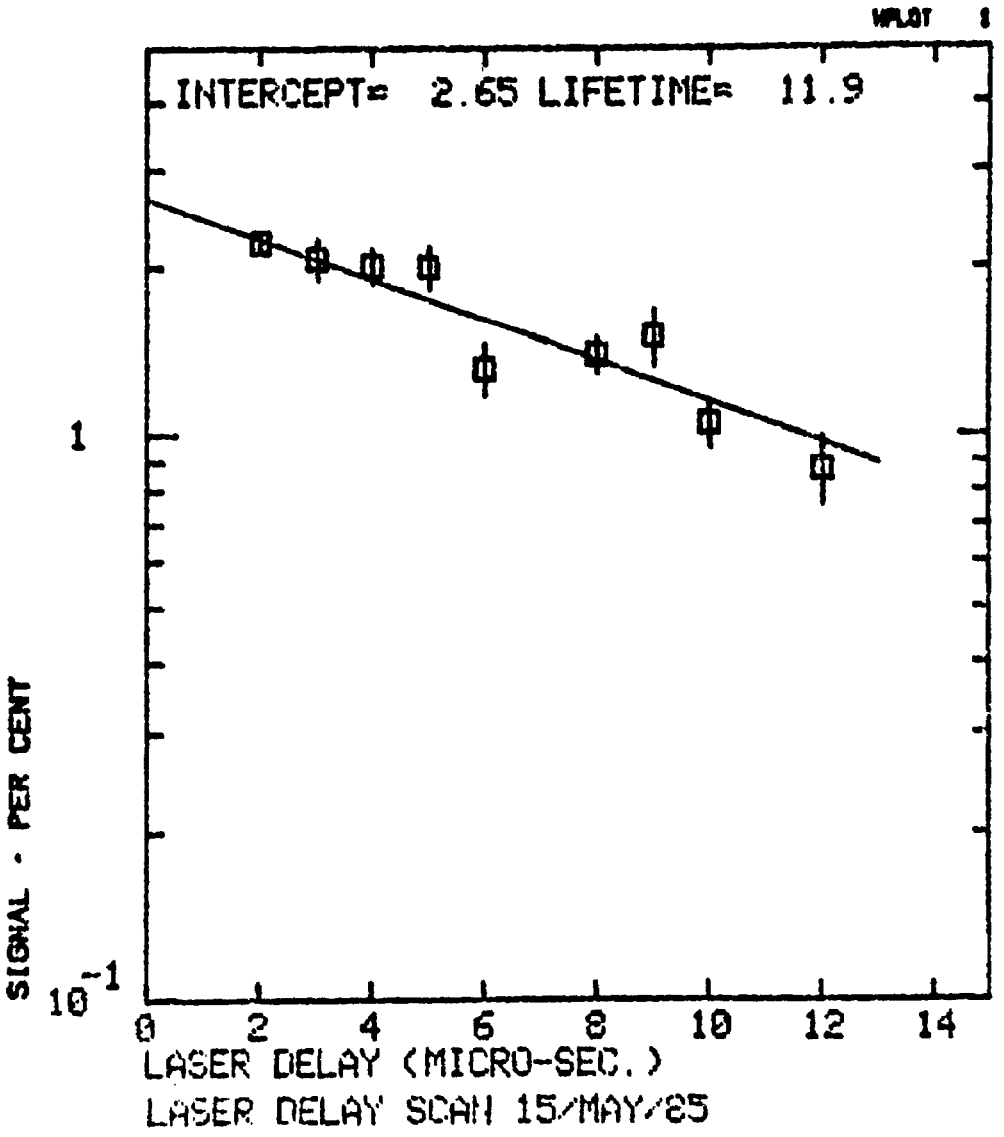

Figure III-8: Dependence of Photoionization Signal on Laser Delay (Fresh Gas Fill)

To obtain light in the visible region, a dye cell pumped by the UV from an excimer laser is used. The dye cell has an efficiency of only about 10%. The excimer laser has an efficiency of ~2% (dependent on the type of gas used) so the net efficiency for excimer plus dye cell is about 0.2%. To obtain the high power levells that may be required for efficient photoionization of negative ions in the streamer chamber, it would be advantageous to be able to use the beam from the excimer laser directly. However, it is highly likely that the beam from a XeCl excimer laser (λ=308 nm) will produce unacceptable background ionization any of residual contaminant organic gas. We decided to investigate use of the excimer laser with a XeF fill (λ=351 nm). This wavelength is considerably longer than the 308 nm of a XeCl fill and is also somewhat longer than the 337 nm from a nitrogen laser which other groups have used to photoionize residual contaminant gas in PWC's and drift chambers. Thus one expects considerably less background ionization. Further (Table III-2) the photoionization cross section for oxygen negative ions should be higher at 351 nm than at 408 nm.

In June of this year we measured a photoionization signal of 26% with a XeF excimer laser. Figure III-9 shows a typical negative ion lifetime curve taken with this beam. There was a small background ionization associated with beam halo striking the ion chamber electrodes. This background "cleaned up" after running the laser into the chamber for a while, and in any case was at a tolerable level for the streamer chamber application.

To summarize the results on photoionization:

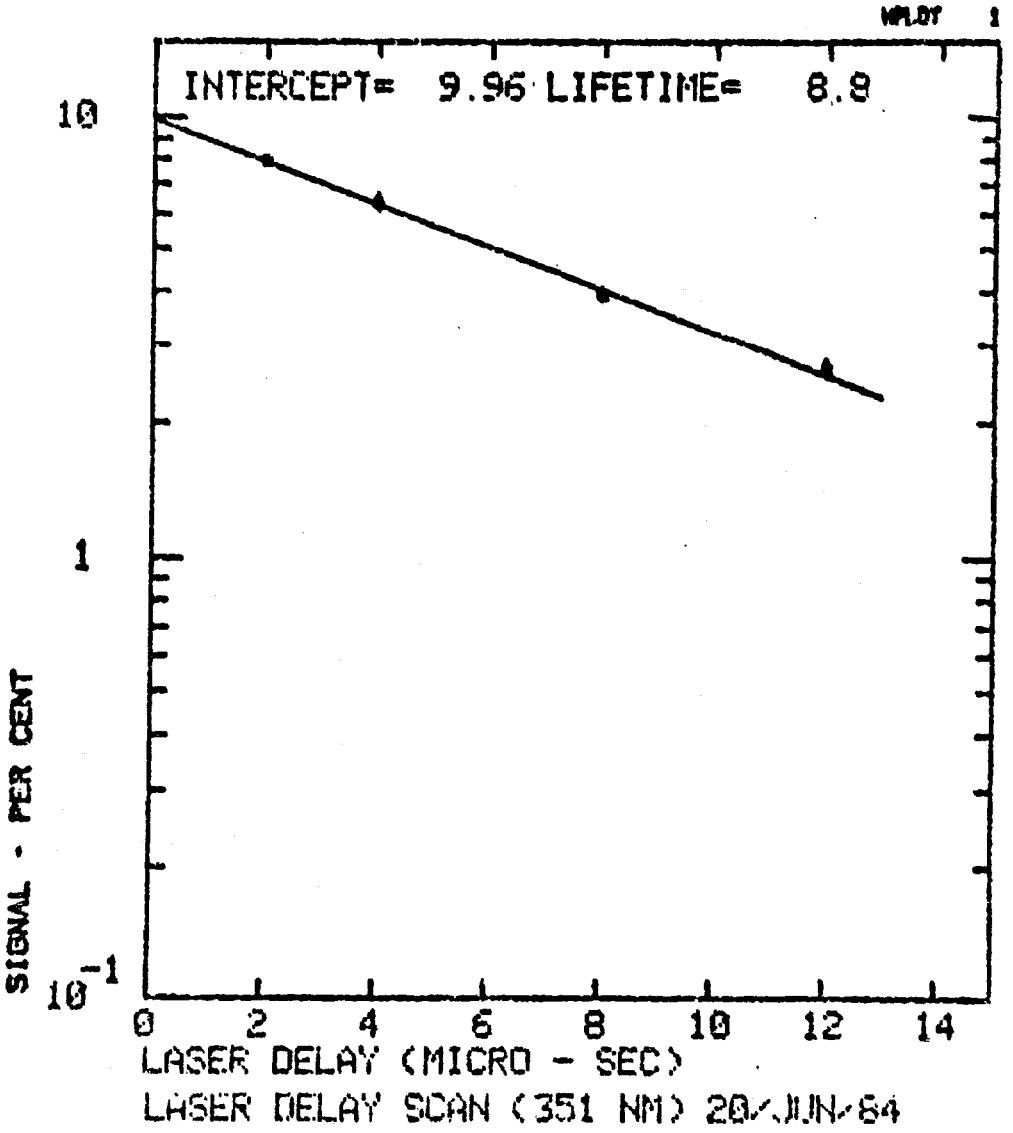

Figure III-9: Photoinization Signal verses Laser Delay for 351 nm Beam

With 406 nm light:

1. The observed signal for 120 mJ/cm^2 is 2.6% of the α signal. Unfolding the geometric overlap of the laser beam with the ionization, this corresponds to 18% photoionization efficiency.

2. Adding 100 μm Hg partial pressure CO_2 kills the photoionization signal.

3. The photoionization signal size is linear with laser power.

With 351 nm light:

1. The observed signal for 125 mJ/cm^2 is 25.8% of the α signal. Unfolding the geometric overlap of the laser beam, this corresponds to 43% photoionization efficiency.

2. There may be a small photoionization signal (≤ 3%) from CO_4^- (we can only set an upper limit). This would represent an unacceptably high background in a streamer chamber in a beam if one allowed the CO_4^- to "disappear" only by diffusion to the walls (~ few seconds to ~ few minutes for this to occur). A modest drift field will remove the CO_4^- in a few milliseconds however.

For both wavelengths (351 nm and 408 nm) we have observed negative ion lifetimes (chamber memory time) which are adequate for use in the streamer chamber. The memory time can be controlled by controlling the carbon dioxide concentration in the gas.

The following directions have been indicated by the ion chamber research:

1. A recirculating purifier (cold trap) should be included in the streamer chamber gas system. We are currently purchasing and fabricating pieces of this system. We expect to be able to test the performance of the gas system using the ion chamber by the end of this year.

2. A carbon dioxide monitor capable of measuring partial pressures of ~ 1 micron Hg carbon dioxide in 100 atm buffer gas should be included in the gas system. Commercially available infrared spectroscopes have this sensitivity. We have ordered a 100 atm sample cell and a commercial spectroscope which will be able to measure CO_2 levels down to 1μm Hg partial pressure.

3. A 1-2 Joule XeF excimer laser should be adequate for

photoionizing negative oxygen ions in the new streamer chamber. Such a laser is similar to ones now available commercially. We have located a company that can supply such a laser.

4. A D.C. clearing field may be required on the streamer chamber to eliminate CO_4 ions at a high enough rate. We have a design for an A.C. coupled terminator for the chamber which would allow the use of a clearing field if one is required.

New Pulser

In order to operate a chamber of the size we want (10x5x1.5 cm^3) at ~60 atmospheres, we need a pulser capable of producing ~500 kV pulses into 40Ω with pulse width in the 1-5 ns range. During the past year we have completed the construction and assembly of a conical coaxial Blumlein pulser and tested the pulser up to 250kV. The pulser shows significantly improved rise time (~0.6ns) over the parallel plate pulser used in E630. This rise time means that for the current pulse width (1.5nsec.) the output oltage reaches the full applied voltage.

The research on holographic recording of streamers done here and at CERN indicates that it may be desirable to have a longer high voltage pulse. Design has been completed for a "pseudo-conical" Blumlein network which will fit into the existing pulser and should give almost twice the pulse length (and also improved rise time). This network is currently being fabricated and should be ready for testing by the end of the year.

An important feature of the new pulser, and of the new chamber system, is a high level of modular construction, which should allow much easier access to various components for maintenance or design changes.

In addition to the streamer chamber and pulser, several other pieces will

be required for a full system. These are: a dielectric pressure seal which will allow the pulser and streamer chamber to operate at different pressures; a coaxial to parallel plate transition section which will carry the high voltage pulse from the pulser (coaxial) to the streamer chamber (parallel plate); a high frequency matched termination for the parallel plate line.

The heavy pieces (steel flanges, steel pipe) for the pressure vessels for these sections above have been ordered so that fabrication can begin. Construction has started on the coax-parallel plate transition and design is in progress fo the other pieces.

REFERENCES

[1] L.L.Chau and W.Y.Keung.
Phys.Rev.D, Vol 29,P 592, 1984.

[2] G.H.Trilling.
Physics Reports, Vol 75, P 57, 1981.

[3] Peter S. Cooper.
Miss Distance Distribution.
Yale University Accelerator Group Internal Note, August 5, 1981.

[4]
Mark III results presented at Leipzig Conference and W.Toki, private communication.

[5] N.F.Reay.
Proceedings of the 1983 International Symposium on Lepton and Photon Interactions at High Energies, Cornell University, August 4-9, 1983.

[6] S.Stone.
Proceedings of the 1983 International Symposium on Lepton and Photon Interactions at High Energies, Cornell University, August 4-9, 1983.

[7] A. Vorobyov.
E715 Hyperon Notes 143, 144.
unpublished.

[8] A. Diament-Berger et. al.
Phys. Rev. Lett., Vol 43, p 1774, 1979.

(9) AIP.
AIP Conference Proceedings No. 98, 1983.

[10] W. Bacino et. al.
Phys. Rev. Lett., Vol 42,P 749, 1979.

[11] B. Alper et. al.
Nucl. Phys. B, Vol 100B, P 237, 1975.

[12] L. Tzeng.
Measurement of the Hadronic Production Cross Section in a High Resolution Streamer Chamber Experiment, Ph.D. Thesis,1984,unpubl.
P. McBride.
A Study of the Properties of Muons Produced in the Decays of Charmed Particles, Ph.D. Thesis,1984,unpubl.

[13] L. Tzeng et al.,"$D\bar{D}$ Production in Neutron-Nucleon Interactions,"submitted to Phys. Rev. Lett.

[14] E. J. Wolin.
HQS Measurement Monte Carlo Note - Preliminary report.
Yale University Internal Report 4/23/84.

[15] H. Dreverman.
private communication.

[16] H. Dreverman.
Talk Presented at the Pisa Conference on Instrumentation in High Energy Physics Castiglione del Mare Italy.
1983

[17] Spindler and Hoyer.
Werk fur Feinmechanik und Optik, D-3400 Gottingen, Konigsallee 23, Postfach 122, W. Germany.

[18] Built by Sincroni.
54 avenue de Scheut, B-1070 Bruxelles, Belgium.

[19] W. Schneeberger A.G.
4914 Roggwil BE, Switzerland.

[20] A. Steinmeyer.
P.O.B. 328, D-7470 Albstadt 1 - Ebingen (Wurtt.) W. Germany.

[21] Heidenhain.
Postfach 1260, D-8225 Traunrent, W. Germany.
[22] P. Lecoq and P.Olivier.
Preliminary tests for a first generation holographic experiment, Proceedings of a meeting on the Application of Holographic techniques to bubble chamber physics.
RL81.042 Ed. by R. L. Sekulin.
[23] Cerco.
Zone Industrielle de Courtaboef, av. de la Baltique, F-91940 Les Ulis, France.
[24] SpectraPhysics.
3333 North First Steet, San Jose, California 95134, USA.
[25] Buffam et al.
CERN/EF/INSTR 79-4,1979.
[26] MIK11-2C.
Camac Crate Controller, Standard Engineering, 44800 Industrial Drive, Fremont, California 94538, USA.
[27] Artus.
Boite Postale 9, F-49240 Avrille, France.
[28] Sen-electronique.
31 av. Ernest-Pictet,Geneve, Switzerland.
[29] A. Herve et al.
Nucl. Instr. and Meth.,vol. 202,p. 417,1982.
[30] J.L. Benichou et al.
Nucl. Instr. and Meth.,vol. 214,p. 245, 1983.